ACS Catalysis

RESEARCH ARTICLE

pubs.acs.org/acscatalysis

Mechanism of Methanol Synthesis on Cu through CO_2 and CO Hydrogenation

L. C. Grabow and M. Mavrikakis*

Department of Chemical and Biological Engineering, University of Wisconsin, Madison, Wisconsin 53706, United States

Supporting Information

ABSTRACT: We present a comprehensive mean-field microkinetic model for the methanol synthesis and water-gas-shift (WGS) reactions that includes novel reaction intermediates, such as formic acid (HCOOH) and hydroxymethoxy (CH_3O_2) and allows for the formation of formic acid (HCOOH), formaldehyde (CH_2O), and methyl formate ($HCOOCH_3$) as byproducts. All input model parameters were initially derived from periodic, self-consistent, GGA-PW91 density functional theory calculations on the Cu(111) surface and subsequently fitted to published experimental methanol synthesis rate data, which were collected under realistic conditions on a commercial $Cu/ZnO/Al_2O_3$ catalyst. We find that the WGS reaction follows the carboxyl (COOH)-mediated path and that both CO and CO_2 hydrogenation pathways are active for methanol synthesis. Under typical industrial methanol synthesis conditions, CO_2 hydrogenation is responsible for ~2/3 of the methanol produced. The intermediates of the CO_2 pathway for methanol synthesis include HCOO*, HCOOH*, CH_3O_2*, CH_2O*, and CH_3O*. The formation of formate (HCOO*) from CO_2* and H* on Cu(111) does not involve an intermediate carbonate (CO_3*) species, and hydrogenation of HCOO* leads to HCOOH* instead of dioxymethylene (H_2CO_2*). The effect of CO is not only promotional; CO* is also hydrogenated in significant amounts to HCO*, CH_2O*, CH_3O*, and CH_3OH*. We considered two possibilities for CO promotion: (a) removal of OH* via COOH* to form CO_2 and hydrogen (WGS), and (b) CO-assisted hydrogenation of various surface intermediates, with HCO* being the H-donor. Only the former mechanism contributes to methanol formation, but its effect is small compared with that of direct CO hydrogenation to methanol. Overall, methanol synthesis rates are limited by methoxy (CH_3O*) formation at low $CO_2/(CO + CO_2)$ ratios and by CH_3O* hydrogenation in CO_2-rich feeds. CH_3O* hydrogenation is the common slow step for both the CO and the CO_2 methanol synthesis routes; the relative contribution of each route is determined by their respective slow steps $HCO^* + H^* \rightarrow CH_2O^* + *$ and $HCOOH^* + H^* \rightarrow CH_3O_2^* + *$ as well as by feed composition and reaction conditions. An analysis of the fitted parameters for a commercial $Cu/ZnO/Al_2O_3$ catalyst suggests that a more open Cu surface, for example, Cu(110), Cu(100), and Cu(211) partially covered by oxygen, may provide a better model for the active site of methanol synthesis, but our studies cannot exclude a synergistic effect with the ZnO support.

KEYWORDS: methanol synthesis, water-gas-shift, Cu surfaces, CO_2 hydrogenation, formic acid, density functional theory, microkinetic modeling, reaction mechanism, rate-limiting step

INTRODUCTION

With the increasing cost of energy and the fast depletion of fossil fuels, it is evident that new ways for energy production need to be explored and realized in the near future. The most promising primary energy sources with negligible CO_2 emissions are biomass, nuclear, hydro, wind, and solar power. A new method using a concentrated solar-power-driven heat engine based on reactive metal oxides allows for efficient splitting of water into H_2 and O_2 as well as the production of CO and O_2 from CO_2.[1] CO may be used to generate additional hydrogen via the water-gas-shift (WGS) reaction ($CO + H_2O \rightarrow CO_2 + H_2$). Hydrogen can act directly as a secondary energy carrier, and its energy can be recovered as needed using hydrogen fuel cells. Although the development of highly efficient fuel cells is fairly advanced, there exist several significant hurdles for the widespread use of hydrogen fuel cells in automotive and other mobile applications. As an alternative, CO_2 and H_2 can be used to synthesize methanol. Methanol is produced on an industrial scale from mixtures of $CO/CO_2/H_2$ (synthesis gas) over a $Cu/ZnO/Al_2O_3$ catalyst at typical reaction conditions of 230−280 °C and 50−120 atm.[2] Methanol can be used as a transportation fuel in either modified internal combustion engines or direct methanol fuel cells. In addition to acting as an energy carrier, methanol is

Received: February 3, 2011
Published: March 04, 2011

also a main building block for the production of other important chemicals, such as olefins and aromatics, and offers a very favorable route for chemical fixation of CO_2.[3,4] In light of the numerous advantages of methanol over pure hydrogen as a transportation fuel, the feasibility of a sustainable methanol-based economy has been championed by Olah et al.[5]

Despite the fact that industrial methanol synthesis technology has been in place for almost 100 years, several key mechanistic questions have not been settled. CO hydrogenation ($CO + 2H_2 \rightarrow CH_3OH$) was assumed to be the main reaction pathway for methanol synthesis[6,7] until the isotope labeling experiments by Chinchen et al. strongly suggested that CO_2 is the main carbon source ($CO_2 + 3H_2 \rightarrow CH_3OH + H_2O$).[8] Since Cu is also an excellent WGS catalyst facilitating the conversion of CO to CO_2 and vice versa, the controversy about the carbon source in methanol synthesis still lives on, but the majority of researchers nowadays are in favor of CO_2 hydrogenation mechanisms (for example, see refs 9 and 10).

The controversy is enhanced regarding the nature of the methanol synthesis active site in $Cu/ZnO/Al_2O_3$ catalysts. It has been suggested that ionic Cu^+ sites are the active catalytic centers,[7,11] but on the other hand, linear scaling of the catalyst activity with the metallic Cu area has been reported.[12] Further evidence supporting metallic Cu as the active site is provided by experiments on single crystal Cu(100),[13,14] Cu(110),[15] and polycrystalline Cu films exposing primarily Cu(111) facets.[16] These experiments indicate that the reaction is structure-sensitive and shows turnover frequencies (TOF) for methanol synthesis that are comparable to the industrial catalyst.[14] Fujitani et al. also observed structure sensitivity during the deposition of Zn on single-crystal Cu surfaces: 0.19 ML Zn on Cu(111) results in a 13-fold increase in the methanol synthesis TOF,[17] whereas Zn on Cu(110) acts as a poison.[18] In addition to the structure sensitivity, these results indicate a synergistic effect between the ZnO support and metal Cu particles, adding to the complexity of the reaction mechanism and the nature of its active site.

It has been speculated for a long time how the ZnO support influences the activity for methanol synthesis, and a large number of possibilities have been suggested. Chinchen et al. found Cu supported on SiO_2 and MgO as active as Cu on ZnO and argue that no significant support effect exists.[12] ZnO may allow for the incorporation of Cu^+ ions into the ZnO lattice and thereby stabilize Cu^+.[7] Spillover mechanisms between Cu and ZnO involving migration of H/OH[19] and formate[20] have also been proposed. As suggested by Frost, a Schottky junction effect between Cu and ZnO may increase the number of O vacancies in ZnO by 3 orders of magnitude.[21] Although these defect sites are the active sites when ZnO alone is used as a catalyst, no key reaction intermediates are observed on ZnO when Cu is present, and the junction effect therefore cannot explain the increased activity of Cu/ZnO over Cu alone.[9] Last, it has been unambiguously shown with atom-resolved TEM that ZnO induces shape changes of supported Cu particles, depending on the oxidation and reduction potential of the surrounding gas phase.[22] Under reducing conditions, such as those encountered during methanol synthesis, and at a total pressure of 1.5×10^{-3} bar, Cu particles primarily expose Cu(111) and Cu(100) facets.[22] Dynamic morphology changes and variations in surface area of Cu particles have been taken into account in a previous microkinetic model, and it was shown that the model is significantly improved by including the structure sensitivity on the Cu(111), Cu(100), and Cu(110) facets.[23] However, Ovesen et al.[23] used estimated parameters to describe the interfacial energies used for the Wulff construction of the Cu particles under different atmospheres and found, in contradiction to the TEM work by Hansen et al.,[22] a larger fraction of the Cu(110) facet under reducing conditions. A new, promising approach using TEM in combination with a microelectromechanical system (MEMS) enables atomic-resolution microscopy at ambient pressures and may, in the future, clarify the catalyst particle shape under realistic methanol synthesis conditions.[24]

In addition to the microkinetic model by Ovesen et al., which is the only microkinetic model in the literature including structural changes, several other authors have presented kinetic models for methanol synthesis.[13,14,25−29] All of these kinetic models adequately describe experimentally measured rates, although different assumptions regarding the mechanism and the rate determining step are made. In an attempt to resolve this unsatisfying status quo of kinetic models for methanol synthesis and to address some of the open questions regarding the mechanism and the nature of the active site, we develop here a comprehensive microkinetic model based only on elementary steps investigated by rigorous density functional theory (DFT) calculations. DFT has been shown to be very useful in unraveling multiple aspects of heterogeneous catalysis on transition metal surfaces.[30,31] We primarily address CO_2 hydrogenation as a method for CO_2 fixation, but we also include various CO and CO_2 hydrogenation pathways, the WGS reaction, and the formation of possible byproducts and intermediates, such as formic acid (HCOOH) and formaldehyde (CH_2O). All input parameters for this model are derived from extensive DFT calculations, and no assumptions regarding the rate-limiting step or mechanism are made. We find the experimental evidence that Cu is mainly responsible for the observed methanol synthesis activity of the industrial catalyst convincing and neglect support effects. Since it was shown that under reducing conditions at low pressures, the Cu(111) and Cu(100) surface are predominantly exposed,[22] we chose the Cu(111) surface for our DFT calculations to derive initial guesses for all surface reaction energetics.

METHODS

Density Functional Theory (DFT). All calculations were performed using the DACAPO total energy code.[32,33] The Cu(111) surface is represented by a three-layer slab, periodically repeated in a super cell geometry with five equivalent layers of vacuum (~10.6 Å) between any successive metal slabs. As done previously, we kept the Cu atoms fixed in their bulk truncated positions, since surface relaxation effects in this system are small.[34−36] To accommodate larger coadsorbed species without significant interaction across repeated unit cells, we employ a $p(3 \times 3)$ unit cell, corresponding to a surface coverage of 1/9 ML for each single adsorbate. Adsorption is allowed on only one of the two surfaces exposed, and the electrostatic potential is adjusted accordingly.[37,38] Ultrasoft Vanderbilt pseudopotentials[39] were utilized to describe core electron interactions, and the Kohn−Sham one-electron valence states are expanded on the basis of plane waves with kinetic energy below 25 Ry. The surface Brillouin zone is sampled at 54 special k points; convergence is confirmed with respect to the k point set. The self-consistent PW91 generalized gradient approximation (GGA-PW91)[40,41] was used for describing the exchange-correlation energy and potential. The self-consistent PW91 density is determined by iterative diagonalization of the Kohn−Sham

Hamiltonian, Fermi population of the Kohn−Sham states (k_BT = 0.1 eV), and Pulay mixing of the resulting electron density.[42] All total energies have been extrapolated to k_BT = 0 eV. We calculated the lattice constant for bulk Cu to be 3.66 Å, in good agreement with the experimental value of 3.62 Å.[43] All binding energies (BE) are given with respect to the clean slab and the adsorbate in the gas phase. In the discussion of the DFT results, we refer to electronic energy values neglecting zero point energy (ZPE) corrections unless otherwise noted. For the microkinetic model, we included ZPE corrections, temperature-dependent heat capacity at constant pressure (C_p) corrections and entropy contributions, all derived from calculated vibrational frequencies (see Supporting Information). Frequencies are calculated using the harmonic oscillator assumption by diagonalization of the mass-weighted Hessian matrix in internal coordinates obtained with a displacement of 0.01 Å.[44] Using internal coordinates for the diagonalization of the Hessian matrix allows for separation of translational and rotational modes from the pure vibrational modes.[45] Although it is easy to define the translational and rotational modes for a gas phase species using its center of mass (COM) and principle moments of inertia, it is much harder to unambiguously define these frustrated modes for adsorbed species. Hence, we treat only the two frustrated translational modes of adsorbed species characterized by changes of position of the COM within the plane parallel to the substrate surface separately. Vibrational and frustrated rotational modes are then obtained by diagonalization of the remaining Hessian matrix.

Minimum energy paths and respective activation energy barriers for all elementary steps are calculated using the climbing image nudged elastic band method (CI-NEB).[42−44] The minimum energy path for each elementary step is discretized by at least seven images, including the initial and final state. Transition states were confirmed by vibrational frequency calculations yielding a single imaginary frequency along the reaction coordinate.

Microkinetic Model. We present an extensive microkinetic model[46,47] for methanol synthesis, including WGS, on the basis of 49 elementary steps, taking into account possible formation of byproducts such as formaldehyde, formic acid, and methyl formate. No assumptions regarding the mechanism or the rate-limiting step are made, and with the exception of sticking coefficients, all model parameters are rigorously derived from DFT calculations and later fitted to reproduce published experimental kinetic data collected under realistic conditions on a Cu/ZnO/Al_2O_3 catalyst. Mean-field microkinetic models, as used here, can fail to describe the correct surface kinetics when local ordering is important and diffusion is slow. In these cases, one has to resort to kinetic Monte Carlo (kMC) simulations, which are capable of accounting for the correct local structure and coverage[48] and yet are much more costly if performed properly. To achieve the correct description of a reaction network with kMC, one would have to perform orders of magnitude more DFT calculations to account for various adsorbate ensembles surrounding the active site for a certain elementary step,[49] which can be done for simple reaction networks. Unfortunately, to date, such an analysis remains completely impractical for reaction networks as complicated as the one needed to describe this complex problem. In addition, at typical methanol synthesis temperatures (∼500 K), we expect the adsorbates on the surface to be well-mixed and diffusion limitations to be negligible. Hence, the use of a mean-field microkinetic model is justified, and more complex kMC simulations are not necessary.

Lateral adsorbate−adsorbate interactions can influence the stability of intermediates and the kinetics of strong binding metals which exhibit high surface coverages.[50] However, we expect the total surface coverage under typical methanol synthesis conditions to be low, and all binding energies and activation barriers are assumed to be coverage-independent. The maximum surface coverage was restricted to 1 ML, and multilayer adsorption was not considered. For some of the larger species treated in our model, the number of blocked sites cannot be easily defined. For simplicity, we assume that all species occupy exactly one site on the surface.

The entropy was directly calculated from the vibrational frequencies of the respective states and used to fit the parameters of the Shomate equation. To obtain enthalpy estimates for all intermediates, the electronic energy was corrected for zero point energy (ZPE) contributions and temperature variations using C_p.[51] The transition state energies were also corrected using ZPE and C_p corrections in a similar manner. The pre-exponential factor was calculated from entropy differences between the initial and transition states of the respective elementary step.[47] For spontaneous reactions, we assumed a pre-exponential factor of 10^{13} s^{-1}. Instead of fitting transition state energies (i.e., activation barriers) directly, we introduced, as in an earlier publication, a parameter ω, which describes the proximity of the transition state to the initial or final state of the respective elementary step.[52] This parameter ω can be estimated from NEB calculations as the ratio (reaction coordinate (transition state))/(reaction coordinate-(final state)). If the transition state occurs early in the reaction (the reaction coordinate of the transition state is small in comparison to the reaction coordinate of the final state), then ω approaches 0. In contrast, ω = 1 indicates a transition state with final state character. The forward activation barrier E_f is then calculated as $E_f = E_{f,DFT} + \omega(\Delta H - \Delta E_{DFT})$, where $E_{f,DFT}$ and ΔE_{DFT} correspond to the activation energy barrier and energy change derived from DFT and are kept constant throughout. The reaction enthalpy ΔH is calculated from the individual enthalpies of all involved species and depends on the temperature (C_p corrections) according to the Shomate equation. ΔH can also be altered during the fitting process by (de)stabilizing the involved species. Using this approach to calculate the activation energy by varying ω ensures that the fitted barrier remains qualitatively similar to the predicted barrier from DFT calculations. This idea is analogous to the Brønsted−Evans−Polanyi principle for surface reactions in which activation energies are linearly correlated to reaction enthalpies across different transition metals.[53−55] For more details, see the Supporting Information.

RESULTS AND DISCUSSION

To develop a consistent framework for the development of a comprehensive microkinetic model, we have rigorously studied with DFT the properties of 22 adsorbed and 8 gas phase species as well as the reaction energetics of 49 elementary steps. For the presentation of our results, we first focus on the DFT calculations, followed by the results from the microkinetic model. Given the large amount of data, we will not comment on all results in detail; the interested reader can find all relevant data in the tables.

Density Functional Theory Results. We chose a Cu(111) model surface to derive thermodynamic and kinetic parameters for the elementary steps considered. The choice of this surface is motivated by several arguments: (i) the Cu(111) surface is the most thermodynamically stable Cu facet; (ii) TEM experiments

showed that under reducing conditions (such as methanol synthesis), the Cu particles expose primarily Cu(111) and Cu(100) facets;[22] and (iii) measured reaction rates on polycrystalline Cu exposing mostly Cu(111) facets are similar to rates from realistic Cu/ZnO catalysts.[16] Since there is general agreement that methanol synthesis is a structure-sensitive reaction, the choice of the model surface may have significant impact on the results. For this reason, a careful analysis of the kinetic modeling results presented later is required. We studied 49 elementary steps that allow for a wide variety of different reaction mechanisms including the formation of unwanted byproducts. Our microkinetic model reveals that several of the DFT-investigated elementary steps are of little relevance to the overall reaction because of high activation barriers ($\geq$2.0 eV) or extremely low reactant coverages. In the text, we focus only on the key elementary steps that contribute to the overall reaction. Additional data for the remaining elementary steps is included in Tables 1 and 2, Figure 1, and the Supporting Information.

Water-Gas-Shift. Cu/ZnO is not only the catalyst of choice for methanol synthesis, but it is also a highly active catalyst for the low temperature WGS reaction. The typical feed for the methanol synthesis reaction contains CO, CO_2, and H_2, allowing for the conversion of CO_2 and H_2 into CO and H_2O via the reverse WGS reaction. For a correct description of the reaction kinetics, it is therefore necessary to include the WGS reaction in a microkinetic model for methanol synthesis. Gokhale et al.[34] recently studied the WGS reaction mechanism on Cu and found that under typical conditions, the reaction proceeds via a carboxyl (COOH*) intermediate formed from CO* and OH*. COOH* then reacts with surface OH* to form CO_2 and H_2O. The rate-limiting step is H abstraction from H_2O*. The experimentally observed formate species (HCOO*) acts merely as a spectator species. An analogous study of WGS on Pt draws similar conclusions, but in the case of Pt, the concentration of surface OH* is very low, and COOH* decomposes directly to CO_2 and adsorbed H*, which is the rate-limiting step.[52]

In the present model, both pathways and additional routes for the WGS reaction are included (e.g. the direct CO oxidation via R9 (see Table 2), or the link through formic acid (HCOOH) and formaldehyde (CH_2O), which can be both formed from CO and CO_2 hydrogenation). Because all DFT calculations for the methanol synthesis reactions were done on a p(3 × 3) unit cell (1/9 ML), we repeated all WGS calculations, which were done by Gokhale et al.[34] on a p(2 × 2) unit cell (1/4 ML), on the larger p(3 × 3) unit cell. Activation energy barriers, E_a, agree generally well (within 0.1 eV), but the reaction enthalpies, ΔE, show deviations of ~0.2 eV and even up to 0.35 eV for CO adsorption and COOH* + OH* → CO_2* + H_2O*. CO* molecules experience strong repulsive interactions among each other on the surface and the BE(CO) depends strongly on CO* coverage. This coverage effect was approximated by Gokhale et al., and it is to be expected that at lower coverages, as was calculated here (1/9 ML), the interaction of CO with the metal surface is stronger than that at higher coverages (1/4 ML).[34]

Formate. The formate intermediate (HCOO*, Figure 1a) is quite possibly one of the key intermediates in methanol synthesis[56−61] and has been frequently invoked as a possible intermediate for the WGS reaction.[62−66] It has even been suggested that the TOF for methanol synthesis is proportional to the formate surface coverage on Zn/Cu(111) model catalysts.[17] Hence, HCOO* has received much scientific attention, and a large number of experimental[29,67−79] and theoretical[79−83] studies of HCOO* on Cu surfaces exist. All reported experimental evidence of HCOO* on Cu(111) points to the existence of only a bidendate species,[70,77,84] as was found in our DFT calculations. HCOO* binds through both O atoms to top sites of the Cu(111) surface with a BE(HCOO) of −2.68 eV, and the calculated Cu−O distance is d_{Cu-O} = 2.05 Å. The existence of a monodendate HCOO* species as reported by Gokhale et al.[34] using DFT on a p(2 × 2) unit cell of Cu(111) and by a combined IR/TPD study on oxidized Cu/SiO_2[72] could not be confirmed in our Cu(111)-p(3 × 3) unit cell. No stable monodendate HCOO* on Cu(111) could be found at 1/9 ML coverage. Apparently, coverage effects can play an important role in determining structural stability of various adsorbed states.

Surface HCOO* species can be formed in different ways: (i) combination of CO_2* and H*, (ii) combination of CO_2* and H* via a CO_3* intermediate, and (iii) decomposition of formic acid (HCOOH). The combination of CO_2* and H* is the most straightforward approach and has been used in various experimental studies.[67,70,72−75] Although the direct formation mechanism for HCOO* from CO_2* and H* seems likely, there is evidence that the reaction proceeds via a carbonate (CO_3*) intermediate.[58,72,85−87] Indeed, it has been shown using a combination of polarization modulation infrared reflection absorption spectroscopy (PM-IRRAS), electron energy loss spectroscopy (EELS), temperature programmed desorption (TPD), X-ray photoelectron spectroscopy (XPS), and DFT that on Cu deposited on Pt(111) CO_2 dissociates into CO* and O*, then a facile reaction between CO_2* and O* results in the formation of a CO_3* species adsorbed on step sites.[88] The presence of CO_3* is primarily observed on stepped or rough surfaces or flat surfaces with preadsorbed oxygen,[59,72,85,86,88,89] while clean, single-crystal surfaces of Cu(110),[90,91] Cu(100),[92] and Cu(111)[93] have been shown to be unreactive upon adsorption of CO_2.

Our DFT results verify the experimental observation that CO_2 does not adsorb dissociatively on the Cu(111) surface, and therefore, CO_3* species are not formed due to the lack of atomic oxygen on the surface. Although the formation of CO_3* from CO_2* and O* is very facile with a barrier of only 0.34 eV and a small endothermicity of 0.11 eV, the dissociation of CO_2* is highly activated, with a barrier of 1.77 eV and an endothermicity of 1.12 eV. Unless the atomic oxygen species on the surface are generated via another path, the lowest-energy path for the formation of HCOO* from CO_2* on Cu(111) is the direct CO_2* hydrogenation by adsorbed H* atoms (CO_2* + H* → HCOO* + *) with a barrier of only 0.87 eV and an exothermicity of −0.25 eV.

Finally, HCOO* can also be prepared by the decomposition of HCOOH.[65,70,74,76−78,84,94,95] For this step, we obtain an activation energy barrier of E_a = 0.68 eV; and ΔE = −0.23 eV. Kinetic analysis[73,74] and an STM study[70] of HCOO* prepared by HCOOH decomposition and CO_2/H_2 combination showed that the HCOO* species obtained with the two preparation methods were different. In particular, when HCOO* is prepared from CO_2 and H_2 on Cu(111), well-ordered rows can be observed with STM, but there is no ordering when the HCOOH preparation method is used.[70] The difference was attributed to the higher H coverage for the CO_2 and H_2 preparation method. We note that in our DFT calculations, all HCOO* species are identical, regardless of the elementary step responsible for their production.

Dioxymethylene vs Formic Acid. Formate is a very stable reaction intermediate for methanol synthesis on Cu, and its further hydrogenation to methoxy (CH_3O*, Figure 1d) is often

Table 1. Calculated Binding Energies (BE) and Vibrational Frequencies of Gas Phase and Adsorbed Species at Their Preferred Adsorption Site[a]

species	preferred adsorption site	BE/eV	frequencies/cm^{-1}
H_2	gas		4430
CO	gas		2205
CO_2	gas		2469, 1351, 629, 623
H_2O	gas		3940, 3825, 1575
CH_2O	gas		2898, 2821, 1798, 1472, 1204, 1143
HCOOH	gas		3693, 2980, 1725, 1281, 1025, 996, 925, 682, 402
CH_3OH	gas		3804, 3044, 2969, 2822, 1451, 1410, 1361, 1268, 1027, 943, 482, 292
$HCOOCH_3$	gas		3136, 3084, 3016, 2999, 1720, 1435, 1414, 1390, 1288, 1176, 1127, 1094, 987, 842, 537, 367, 160, 133
H*	fcc	−2.43	1013, 862, 862
O*	fcc	−4.25	470, 325, 324
OH*	fcc	−2.80	3820, 405, 405, 369, 194, 193
H_2O*	top	−0.21	3843, 3732, 1538, 364, 320, 149, 83, 77, 60
CO*	fcc	−0.86	1894, 282, 188, 187, 108, 107
CO_2*	physisorbed	−0.08	2453, 1353, 627, 621, 154, 137, 135, 128, 74
CO_3*	bridge−bridge	−3.62	1760, 963, 885, 754, 618, 599, 275, 213, 165, 163, 121, 71
HCO_3*	top−top	−2.48	3791, 1588, 1407, 1191, 1026, 769, 649, 596, 546, 214, 168, 129, 122, 110, 102
HCO*	bridge	−1.18	2866, 1464, 1216, 558, 375, 187, 127, 108, 96
COH*	fcc	−2.57	3689, 1273, 1085, 336, 322, 287, 222, 198, 18
HCOH*	fcc	−1.85	2901, 2677, 1342, 1109, 1104, 768, 344, 296, 223, 151, 75, 71
HCOO*	top−top	−2.68	2965, 1571, 1332, 1309, 984, 733, 305, 237, 233, 136, 124, 98
H_2CO_2*	bridge−bridge	−3.32	2971, 2931, 1439, 1308, 1170, 1059, 979, 861, 577, 337, 328, 218, 179, 166, 21
COOH*	top	−1.52	3739, 1557, 1204, 1122, 664, 575, 372, 246, 173, 139, 117, 106
HCOOH*	top	−0.22	3241, 3012, 1724, 1343, 1283, 1135, 990, 684, 639, 170, 147, 115, 114, 97, 96
CH_2O*	C-top/O-bridge	−0.06	3075, 2983, 1454, 1228, 1140, 827, 521, 307, 159, 150, 115, 85
CH_3O*	fcc	−2.45	3041, 3038, 2963, 1435, 1434, 1404, 1119, 1116, 1002, 265, 185, 169, 139, 128, 75
CH_2OH*	C-bridge/O-top	−0.84	3671, 3031, 2972, 1384, 1291, 1111, 1056, 891, 498, 400, 327, 167, 105, 102, 64
CH_3O_2*	O-bridge/O-top	−2.01	3712, 3016, 2957, 1452, 1344, 1287, 1192, 1050, 996, 875, 556, 407, 299, 245, 148, 109, 102, 95
CH_3OH*	O-top	−0.28	3749, 3092, 3040, 2970, 1444, 1435, 1409, 1293, 1125, 1034, 980, 373, 164, 129, 119, 99, 76, 52
$HCOOCH_3$	physisorbed	−0.10	3139, 3079, 3003, 2992, 1773, 1429, 1422, 1405, 1339, 1199, 1136, 1123, 981, 900, 753, 361, 296, 136, 119, 99, 84, 78, 73, 23
H_2COOCH_3	O-bridge/O-bridge	−1.96	3071, 3023, 2958, 2921, 2887, 1457, 1441, 1419, 1402, 1345, 1192, 1180, 1130, 1120, 1088, 1040, 848, 526, 348, 261, 213, 167, 127, 108, 78, 77, 12

[a] The more negative the BE, the stronger the interaction with the Cu(111) surface. The zero energy reference corresponds to the gas-phase adsorbate at infinite separation from the Cu(111) surface.

believed to be the rate-determining step.[57] However, for the formation of CH_3O* from HCOO*, the formation of two C−H bonds and the breaking of one C−O bond are necessary. It is unlikely that all three bond-making and bond-breaking events occur simultaneously, and a sequential mechanism via less stable surface intermediates is expected. Considering an adsorbed HCOO* species, one can start with breaking the C−O bond to form a formyl (HCO*, Figure 1f) intermediate. The HCO* intermediate is not very stable, which leads to highly unfavorable energetics of this step. C−O bond-breaking in HCOO* is endothermic by 2.18 eV and has a barrier of 2.36 eV. Because the C−O bond-breaking in HCOO* is so expensive, we will not consider this possibility any further. Alternatively, one can start the stepwise hydrogenation at either the C or O atom of the HCOO* species forming dioxymethylene (H_2CO_2*, Figure 1b) or formic acid (HCOOH*, Figure 1g), respectively.

We have calculated the energetics of both processes, and we found that the hydrogenation of the O atom in HCOO* is both kinetically and thermodynamically preferred over the hydrogenation of the C atom. The potential energy surface (PES) of methanol synthesis in Figure 2 clearly shows that HCOOH* is the more stable product of HCOO* hydrogenation. The formation of HCOOH* is only modestly endothermic (ΔE = 0.23 eV) and has a barrier of 0.91 eV, whereas the formation of H_2CO_2* is endothermic by 0.87 eV and has a barrier of 1.59 eV. On Cu(111), HCOOH* binds weakly through the O atom with a BE(HCOOH) of −0.22 eV.

We calculate vibrational frequencies for ν(O−H), ν(C−H), and the asymmetric COO stretch ν_{as}(COO) of 3241, 3012, and 1724 cm^{-1}, respectively. These frequencies are in reasonable agreement with an IR study of HCOOH adsorption on Cu/SiO_2, in which the characteristic HCOOH* features at 299 K and 10^{-7} Torr are reported at 2870 and 1670 cm^{-1}.[94,96]

It is well-known that HCOOH readily decomposes into HCOO* + H* upon adsorption; in fact, HCOOH has been frequently used to deliver HCOO* species on Cu surfaces.[65,70,74,76−78,84,94,95] However, HCOOH* is rarely mentioned in the context of methanol synthesis. One study considers HCOOH* as an intermediate or byproduct in the hydrogenation of HCOO*,[29] and another study suggests that Cu-bound

dx.doi.org/10.1021/cs200055d |ACS Catal. 2011, 1, 365–384

Table 2. The 49 Elementary Steps Included in the Microkinetic Model[a]

no.	reaction	E_{int}/eV IS/FS	ΔE/eV	E_a / eV	sticking probability or pre-exponential factor	ω
R1	$CO_2 + * \rightarrow CO_2*$		−0.08		1	
R2	$H_2 + 2* \rightarrow 2\ H*$		−0.29		1	
R3	$CO + * \rightarrow CO*$		−0.86		1	
R4	$H_2O + * \rightarrow H_2O*$		−0.21		1	
R5	$HCOOH + * \rightarrow HCOOH*$		−0.22		1	
R6	$CH_2O + * \rightarrow CH_2O*$		−0.04		1	
R7	$CH_3OH + * \rightarrow CH_3OH*$		−0.28		1	
R8	$HCOOCH_3 + * \rightarrow HCOOCH_3*$		−0.10		1	
R9	$CO* + O* \rightarrow CO_2* + *$	0.14/0.76	−1.12	0.65	1.195×10^{12}	0.44
R10	$CO* + OH* \rightarrow COOH* + *$	0/0	0.14	0.56	4.667×10^{11}	0.36
R11	$COOH* + * \rightarrow CO_2* + H*$	0.00/0.11	−0.55	1.23	2.326×10^{13}	0.32
R12[b]	$COOH* + OH* \rightarrow CO_2* + H_2O*$	−0.34/0.22	−0.76	0	1.000×10^{13}	0.00
R13	$COOH* + H* \rightarrow HCOOH* + *$	−0.01/0.00	−0.59	0.73	6.793×10^{13}	0.35
R14	$H_2O* + * \rightarrow OH* + H*$	0.01/0.08	0.21	1.39	1.436×10^{11}	0.60
R15	$OH* + * \rightarrow O* + H*$	0.06/0.88	0.72	1.68	2.193×10^{13}	0.88
R16	$2\ OH* \rightarrow H_2O* + O*$	0.15/−0.16	0.51	0.61	1.675×10^{12}	0.65
R17	$CO_2* + H* \rightarrow HCOO* + *$	0.11/0.00	−0.25	0.87	3.658×10^{13}	0.31
R18	$HCOO* + H* \rightarrow H_2CO_2* + *$	0.01/0.00	0.87	1.59	3.737×10^{13}	0.54
R19	$HCOO* + H* \rightarrow HCOOH* + *$	0.01/0.00	0.23	0.91	1.302×10^{14}	0.50
R20	$HCOOH* + H* \rightarrow CH_3O_2* + *$	0.06/0.02	0.10	1.04	6.244×10^{14}	0.45
R21	$H_2CO_2* + H* \rightarrow CH_3O_2* + *$	0.12/0.01	−0.54	0.74	2.114×10^{12}	0.58
R22[c]	$H_2CO_2* + * \rightarrow CH_2O* + O*$	0.00/−0.19	0.91	0.91	1.000×10^{13}	1.0
R23[c]	$CH_3O_2* + * \rightarrow CH_2O* + OH*$	0.00/−0.05	0.74	0.74	1.000×10^{13}	1.0
R24	$CH_2O* + H* \rightarrow CH_3O* + *$	−0.04/0.00	−1.02	0.24	1.815×10^{13}	0.37
R25	$CH_3O* + H* \rightarrow CH_3OH*$	0.06/0.00	−0.23	1.17	1.280×10^{13}	0.60
R26	$CO* + H* \rightarrow HCO* + *$	0.08/0.00	0.78	0.99	9.240×10^{12}	0.61
R27	$CO* + H* \rightarrow COH* + *$	0.08/0.00	1.15	2.26	1.118×10^{13}	0.42
R28	$HCOO* + * \rightarrow HCO* + O*$	0.00/−0.05	2.18	2.36	2.570×10^{12}	0.56
R29	$HCO* + H* \rightarrow HCOH* + *$	0.14/0.00	0.09	0.91	8.971×10^{12}	0.54
R30	$HCO* + H* \rightarrow CH_2O* + *$	0.00/0.02	−0.40	0.47	5.685×10^{12}	0.42
R31	$CH_2O* + H* \rightarrow CH_2OH* + *$	−0.01/0.01	−0.06	0.82	9.518×10^{14}	0.58
R32	$HCOH* + H* \rightarrow CH_2OH* + *$	0.07/0.00	−0.55	0.47	3.698×10^{12}	0.40
R33	$CH_2OH* + H* \rightarrow CH_3OH* + *$	0.01/0.07	−1.19	0.51	8.189×10^{12}	0.32
R34	$HCOOH* + * \rightarrow HCO* + OH*$	0.00/−0.09	1.24	1.63	5.242×10^{12}	0.72
R35	$HCOOH* + * \rightarrow HCOH* + O*$	0.00/0.15	2.04	2.50	4.828×10^{11}	0.70
R36	$CH_3O_2* + * \rightarrow CH_2OH* + O*$	0.02/0.00	1.39	2.01	5.485×10^{13}	0.67
R37	$CO_2* + O* \rightarrow CO_3* + *$	−0.07/0.00	0.11	0.34	8.902×10^{11}	0.47
R38	$CO_3* + H* \rightarrow HCO_3* + *$	0.10/0.52	−1.21	1.00	1.717×10^{13}	0.39
R39[b]	$O*+ HCO* \rightarrow OH*+ CO*$	−0.10/0.17	−1.50	0	1.000×10^{13}	0.00
R40	$OH*+ HCO* \rightarrow H_2O*+ CO*$	−0.10/−0.08	−0.99	0.30	9.597×10^{12}	0.45
R41	$HCOO* + HCO* \rightarrow HCOOH*+ CO*$	−0.04/−0.05	−0.56	0.60	2.200×10^{14}	0.34
R42	$HCOO*+ HCO* \rightarrow H_2CO_2*+ CO*$	−0.04/0.03	0.09	0.80	3.441×10^{12}	0.53
R43	$HCOOH* + HCO* \rightarrow CH_3O_2*+ CO*$	−0.11/−0.03	−0.68	0.42	5.340×10^{11}	0.42
R44[b]	$CH_2O* + HCO* \rightarrow CH_3O*+ CO*$	−0.04/−0.03	−1.81	0	1.000×10^{13}	0.00
R45	$CH_3O*+ HCO* \rightarrow CH_3OH*+ CO*$	−0.05/−0.04	−1.02	0.38	1.934×10^{12}	0.54
R46[d]	$CH_3O* + HCOO* \rightarrow HCOOCH_3* + O*$	−0.10/−0.02	0.99	1.24	6.934×10^{11}	0.80
R47	$CH_3O* + CH_2O* \rightarrow H_2COOCH_3* + *$	−0.12/0.02	−0.78	0.13	6.405×10^{13}	0.58
R48	$HCOOCH_3* + H* \rightarrow H_2COOCH_3* + *$	0.16/0.01	0.01	0.94	1.536×10^{12}	0.54
R49	$2\ CH_2O* \rightarrow HCOOCH_3* + *$	−0.28/0.00	−1.81	1.11	2.527×10^{14}	0.73

[a] Pre-exponential factors are calculated from ΔS^{TS} at 499.3 K. E_{int} describes the adsorbate−adsorbate interactions in the initial (IS) and final states (FS) used in the NEB calculation. ΔE and E_a are the energy change and activation barrier from DFT at infinite separation without further corrections (e.g. ZPE, C_p). ω describes the proximity of the transition state to the initial/final state as described in the Methods section. [b] Reaction is spontaneous: $\omega = 0.0$ and pre-exponential factor = $1 \times 10^{13}\ s^{-1}$ are assumed. [c] Reaction is spontaneous in the reverse direction: $\omega = 1.0$ and pre-exponential factor = $1 \times 10^{13}\ s^{-1}$ are assumed. [d] A stable $HCOOOCH_3*$ is formed as an intermediate, but it is not explicitly included in the microkinetic model. Two NEBs were used to find the transition states of the steps $CH_3O* + HCOO* \rightarrow HCOOOCH_3* + *$ and $HCOOOCH_3* + * \rightarrow HCOOCH_3* + O*$. The reported barrier and pre-exponential factor are obtained from the transition state of the step $HCOOOCH_3* + * \rightarrow HCOOCH_3* + O*$, which has the highest total energy.

dx.doi.org/10.1021/cs200055d |ACS Catal. 2011, 1, 365–384

HCOO* reacts to HCOOH* as a byproduct, and only ZnO-bound HCOO* is further reduced to methanol.[20] On the contrary, isotopic labeling studies showed that CH_3OH could not be synthesized by HCOOH* or HCOO* hydrogenation on Cu/ZrO_2, but only from CH_2O* hydrogenation.[97] An FTIR study on Cu/ZrO_2 arrived at the same conclusion.[98] MS-IR experiments on Cu/SiO_2 and unsupported Cu[99] as well as kinetic modeling indicates that direct hydrogenation of HCOO* does not lead to methanol synthesis.[29] To our knowledge, there is only one mention of HCOOH* as an active reaction intermediate in methanol synthesis from CO_2 and H_2 on $Cu/ZnO/Al_2O_3$.[100]

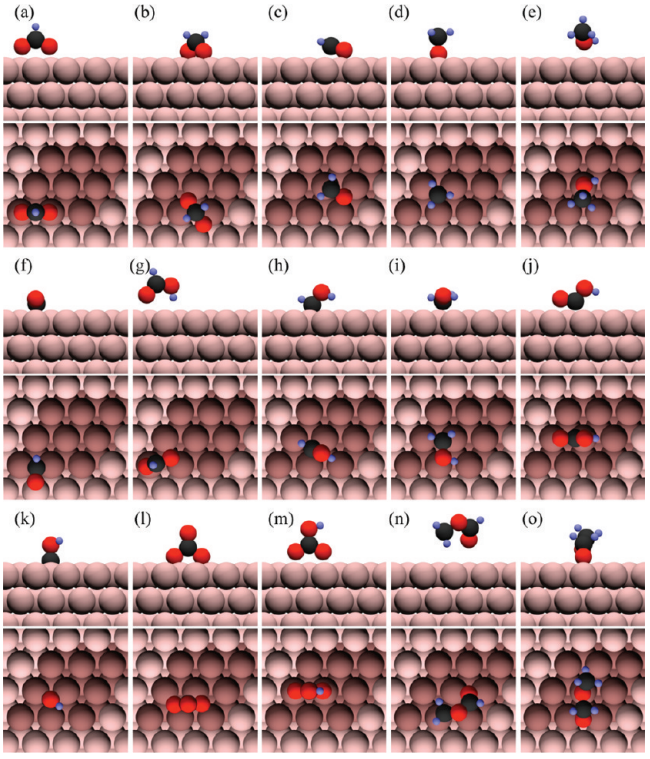

Figure 1. Most stable adsorption states of selected intermediates in the methanol synthesis reaction on Cu(111). Adsorbed states of atomic species, weakly adsorbed molecular species and common species such as OH and CO are not included. Top row: (a) formate, (b) dioxymethylene, (c) formaldehyde, (d) methoxy, (e) methanol. Middle row: (f) formyl, (g) formic acid, (h) hydroxymethylene, (i) hydroxymethyl, (j) carboxyl. Bottom row: (k) hydroxymethylidyne, (l) carbonate, (m) bicarbonate, (n) methyl formate, (o) methoxyoxymethylene.

In stark contrast to HCOOH*, H_2CO_2* has been frequently invoked as the product of HCOO* hydrogenation on Cu.[14,23,25,58,95,101,102] Similar to HCOO*, H_2CO_2* binds with both O atoms to the Cu surface, but the O atoms are in bridge positions, rather than on atop sites, and the C atom is centered above another bridge site (Figure 1b). We calculated the BE(H_2CO_2) as −3.32 eV. Our results for adsorbed HCOO*, H_2CO_2*, and its formation from HCOO* agree well with a previous periodic DFT study.[83] Gomes and Gomes have performed DFT calculations on 7- and 30-atom Cu clusters and reported a cross-bridge adsorption that is ∼0.4−0.7 eV more stable than the aligned-bridge geometry.[81,103] The cross-bridge adsorption was not stable in our periodic slab calculations, and we speculate that Gomes and Gomes's result may be related to the specific cluster used in their study. Increasing the cluster size from Cu_7 to Cu_{30} increases the BE(H_2CO_2) on the cross-bridge site from −4.19 to −4.30 eV and at the same time decreases the BE(H_2CO_2) on the aligned-bridge site from −3.80 to −3.55 eV.[81] Our calculated frequencies in Table 1 show deviations of 30−80 cm^{-1} from the Cu_{30} results of cross-bridge adsorbed H_2CO_2 reported by Gomes and Gomes,[81] but the relative order of the different modes is identical in both calculations.

It was previously suggested that H_2CO_2* may react directly to CH_3O* via the reaction H_2CO_2* + H* → CH_3O* + O*, and this reaction is included in a variety of published kinetic models.[14,23,25,102] However, this concerted step would require the formation of a C−H bond with a simultaneous C−O bond

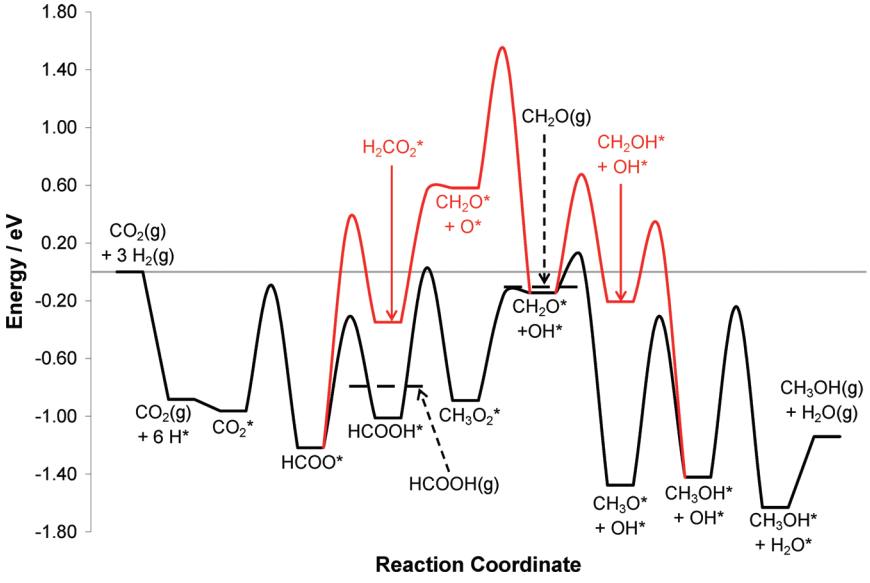

Figure 2. Potential energy surface of methanol synthesis via CO_2 hydrogenation. To improve legibility, H* was omitted from the labels after the adsorption of six H atoms in the first step. The black line indicates the lowest-energy pathway through the HCOO*, HCOOH*, CH_3O_2*, CH_2O*, and CH_3O* intermediates. The main intermediates along the red path are HCOO*, H_2CO_2*, CH_2O*, and CH_2OH*. The two dashed horizontal lines indicate the desorption barriers of HCOOH and CH_2O.

dx.doi.org/10.1021/cs200055d |ACS Catal. 2011, 1, 365–384

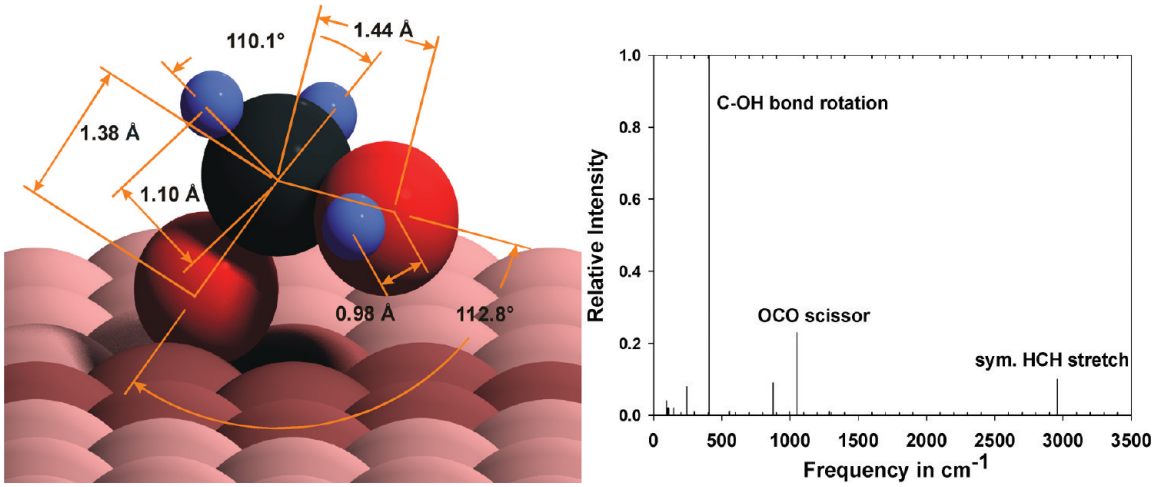

Figure 3. Hydroxymethoxy (CH_3O_2) on Cu(111). (a) Binding geometry (BE = −2.01 eV). (b) Simulated vibrational spectrum.

breaking event. We devoted significant effort in exploring the details of this hypothetical concerted step, but in all cases, our NEB calculations predicted the C−O bond breaking to happen first, forming adsorbed CH_2O^*. CH_2O^* is then hydrogenated to CH_3O^*, but the reaction events are sequential rather than concerted. We therefore concluded that the above surface reaction ($H_2CO_2^* + H^* \rightarrow CH_3O^* + O^*$) cannot be an elementary reaction step and did not include it in the microkinetic model. Importantly, the alternative sequential two-step pathway going through CH_2O^* (reactions R24 and R25 in Table 2) is included in our microkinetic model.

Formaldehyde (CH_2O). The interaction between formaldehyde (CH_2O^*, Figure 1c) and Cu(111) is very weak, characterized by a BE(CH_2O) of −0.04 eV. Hence, if CH_2O^* is formed as an intermediate in methanol synthesis, the observation of CH_2O as byproduct should be expected, but experimental evidence for CH_2O production is not conclusive.[13,14] On the other hand, adsorption of CH_2O on $Cu/ZnO/Al_2O_3$ yields both CH_3O^* and $HCOO^*$ species, which is in support of CH_2O^* as surface intermediate for the reduction of $HCOO^*$.[9,57] In addition, an isotope labeling study for methanol synthesis on Cu/ZrO_2 suggested that CH_3OH is exclusively formed from CH_2O^*, not from $HCOO^*$, and CH_2O^* is the key reaction intermediate in methanol synthesis.[97] Despite the fact that several kinetic models which do not include CH_2O^* as an intermediate[14,23,25,102] have been published, we do include CH_2O^* in our model.

CH_2O^* on the supported Cu catalyst may be more stable than the calculated BE(CH_2O) of −0.04 eV on Cu(111) suggests. On Cu(110), the BE was estimated to be −0.59 eV.[104] Under industrial conditions, the Cu surface of the catalyst is partially oxidized.[12] The presence of oxygen on the Cu(111) surface further stabilizes CH_2O^*. Upon coadsorption of 1/9 ML of O and 1/9 ML of CH_2O^*, the two adsorbates show an attractive interaction of −0.2 eV. Not only the interaction with O^*, but also the interaction of CH_2O^* molecules among themselves is considerable. When two CH_2O^* molecules are adsorbed in a p(3 × 3) unit cell, the attraction between them is ∼−0.3 eV. CH_2O polymerization on Cu (110)[105] and (100)[106] surfaces has also been reported, but we do not consider that phenomenon in our model.

Hydroxymethoxy (CH_3O_2). $CH_3O_2^*$ is a methoxy species in which one H atom is replaced by an OH group, as shown in Figure 3. $CH_3O_2^*$ binds through its O end to Cu(111), with a BE(CH_3O_2) of −2.01 eV. Structural and vibrational properties of this adsorbed state are given in Figure 3 and Table 1. To our knowledge, there exists only one recent publication that considers $CH_3O_2^*$ as an intermediate in methanol synthesis on Cu/ZrO_2.[107]

$CH_3O_2^*$ can be formed by hydrogen addition either to the C atom of $HCOOH^*$ or to an O atom of $H_2CO_2^*$. The hydrogenation of $HCOOH^*$ is quasi-thermoneutral (ΔE = 0.10 eV) with a barrier of E_a = 1.04 eV. The energetics for the formation of $CH_3O_2^*$ from $H_2CO_2^*$ are more favorable (ΔE = −0.54 eV, E_a = 0.74 eV), but we note here again that the total energy of adsorbed $HCOOH^*$ is 0.64 eV lower than the total energy of its isomer adsorbed $H_2CO_2^*$. In the case of $HCOOH^*$, no other competitive pathways for further reaction exist: both possible C−O bond breaking steps are highly activated ($HCOOH^* + * \rightarrow HCO^* + OH^*$: ΔE = 1.24 eV, E_a = 1.63 eV. $HCOOH^* + * \rightarrow HCOH^* + O^*$: ΔE = 2.04 eV, E_a = 2.50 eV), and although these steps are included in the kinetic model, we will not discuss these pathways in greater detail here.

For $H_2CO_2^*$, the situation is somewhat different. In addition to the very favorable hydrogenation to $CH_3O_2^*$, its reduction to CH_2O^* is an alternative. C−O bond-breaking in $H_2CO_2^*$ has only a thermodynamic barrier (ΔE = 0.91 eV, E_a = 0.91 eV); in other words, the recombination of $CH_2O^* + O^*$ to $H_2CO_2^*$ is spontaneous. Spontaneous formation of $H_2CO_2^*$ from $CH_2O^* + O^*$ has also been reported in a DFT study on Cu(110).[108] Similarly, the recombination of $CH_2O^* + OH^*$ to $CH_3O_2^*$ is spontaneous, which opens up a low-energy pathway for the C−O bond breaking in $CH_3O_2^*$. The reaction $CH_3O_2^* + * \rightarrow CH_2O^* + OH^*$ is endothermic with ΔE = 0.74 eV (E_a = 0.74 eV). In summary, we suggest, on the basis of our DFT results alone, that the reduction of $HCOO^*$ to CH_2O^* may proceed via the sequence $HCOO^* + 2\,H^* \rightarrow HCOOH^* + H^* + * \rightarrow CH_3O_2^* + 2^* \rightarrow CH_2O^* + OH^* + *$.

Methoxy (CH_3O) vs Hydroxymethyl (CH_2OH). The last intermediate for stepwise hydrogenation of CH_2O^* to CH_3OH is either methoxy (CH_3O^*) or its isomer hydroxymethyl (CH_2OH^*). In both pathways to CH_3OH, one C−H bond and one O−H bond needs to be formed, but in different order. The activation energy barriers in the CH_2OH^* pathway ($CH_2O^* \rightarrow CH_2OH^* \rightarrow CH_3OH^*$) are E_a = 0.82 eV for the O−H bond-making and E_a = 0.51 eV for the C−H bond-making. For the

dx.doi.org/10.1021/cs200055d |ACS Catal. 2011, 1, 365–384

Table 3. Comparison of Experimental[115] and Calculated Methyl Formate Frequencies[a]

vibrational mode	EELS frequency/ cm^{-1} Cu(110)[115]	DFT frequency/ cm^{-1} Cu(111)
COC bend	370	296
OCO bend	720	753
OCO sym. stretch	920	900[b]
methyl rock	1180	1123, 1136
OCO asym. stretch	1260	1199[c]
methyl bend	1450	1405, 1422, 1429
C═O stretch	1670	1773
CH stretch	2980	2992, 3003, 3079, 3139
	3050	

[a] Note the different Cu facets for the two columns. [b] O−CH3 stretch. [c] COC asym. stretch.

CH_3O^* pathway, the barriers are E_a = 0.24 eV and E_a = 1.17 eV, for the C−H and O−H bond-making, respectively. A graphical representation of both pathways is given in the PES in Figure 2, where it can be seen that even though the CH_3O^* pathway has the highest individual barrier (E_a = 1.17 eV) for the final hydrogenation step, its energy trace lies permanently lower than the energy trace for the CH_2OH^* pathway. This reflects the much higher stability of adsorbed CH_3O^* as compared with adsorbed CH_2OH^*. The difference in total energy of the two isomers is 0.96 eV. The higher stability of CH_3O^* leads to a higher surface coverage compared with CH_2OH^*, and the abundance of CH_3O^* species on the surface counteracts the high activation barrier for its last hydrogenation step. An in situ FTIR study on Cu/ZnO and Cu/ZnO/Cr_2O_3 catalyst concluded that CH_3O^* hydrogenation is the rate-limiting step in methanol synthesis,[109] which agrees with the high barrier calculated here. Overall, the DFT results imply that the CH_3O^* pathway is dominant over the CH_2OH^* pathway. Further support for CH_3O^* as the final reaction intermediate prior to CH_3OH formation has been provided previously by a large number of experimental studies. CH_3O^* was identified in situ using FTIR on Cu/ZnO/Al_2O_3,[60] Cu/ZnO,[66,69] CuO/ZnO,[109] Cu/SiO_2,[87,110] and Cu/ZrO_2.[87,98,111] The reverse process, adsorption of methanol, is well-known to be dissociative on Cu(110)[104] and on most transition metals[112] and results in the formation of adsorbed CH_3O^*.

Methyl Formate ($HCOOCH_3$). In-situ FTIR studies have identified methyl formate ($HCOOCH_3$, Figure 1n) under methanol synthesis conditions,[87] and it is a major byproduct of methanol decomposition over Cu/SiO_2.[113] The adsorption of $HCOOCH_3$ on Cu/ZnO/SiO_2[114] and Cu(110) predosed with O*[115] leads to the formation of $HCOO^*$ and CH_3O^* species. Since $HCOOCH_3$ did not react on the clean Cu(110) surface but only when O* was predosed, Sexton et al. suggested that $HCOOCH_3^*$ dissociates in the step $HCOOCH_3^* + O^* \rightarrow CH_3O^* + HCOO^*$.[115] The discovery of alcohol-promoted pathways for the low-temperature methanol synthesis provides further motivation for the investigation of $HCOOCH_3$.[116−120] In these reaction schemes, HCOOH* or $HCOO^*$ is synthesized from CO_2 and H_2, followed by the esterification with ethanol/propanol to ethyl/propyl formate. Hydrogenolysis of the alkyl formates recovers the alcohol promoter and produces methanol. Recently, Yu et al. proposed a method for CO_2 fixation by reaction with H_2 in the presence of CH_3OH over clean and promoted Cu/ZnO/Al_2O_3 catalysts to form $HCOOCH_3$.[121] It is clear that $HCOOCH_3$ is closely related to methanol synthesis intermediates, and the observation that it decomposes in the presence of oxygen into $HCOO^*$ and CH_3O^* upon adsorption makes it a potential reaction intermediate connecting $HCOO^*$ and CH_3O^*.

A monolayer of $HCOOCH_3^*$ on Cu(110) at 140 K was characterized using EELS.[115] As shown in Table 3, our calculated frequencies for $HCOOCH_3^*$ on Cu(111) are in general good agreement with these EELS data on Cu(110). Our results disagree on only the mode assignment for frequencies at 920 and 1260 cm^{-1}. There is no indication of any OCO stretching modes, but similar modes with frequencies at 900 and 1199 cm^{-1} exist. These modes are an O−CH_3 stretch and an asymmetric (asym) COC stretch, respectively.

The decomposition of $HCOOCH_3^*$ into two CH_2O^* molecules turns out to be very unfavorable and highly activated on Cu(111). The reaction is endothermic (ΔE = 1.81 eV) and has a barrier of E_a = 2.92 eV. This step is concerted (formation of a C−O and a C−H bond while breaking another C−H bond), and the transition state has, indeed, a single imaginary frequency. The reverse reaction ($2\ H_2CO^* \rightarrow HCOOCH_3^* + *$) is very exothermic and has a modest barrier of 1.11 eV. However, Sexton et al. did not find any evidence for $HCOOCH_3^*$ formation from CH_2O^* on Cu(110); instead, CH_2O^* formed a surface polymeric structure.[115] We did not consider CH_2O^* polymerization in our study, but we find that CH_2O^* has other much more facile reaction channels it can follow than its dimerization to $HCOOCH_3^*$. For example, CH_2O^* spontaneously reacts with adsorbed O* and OH* to give $H_2CO_2^*$ and $CH_3O_2^*$, respectively, and these two reactions were included in our microkinetic model.

CO Promotion. The promotional effect of CO on methanol synthesis from CO_2/H_2 mixtures is experimentally well established, but the exact origin remains unknown. There is convincing evidence that the gas phase reduction potential determined by the CO concentration induces morphological changes on the catalyst particles that can be responsible for changes in the catalytic activity.[22,23,102] Furthermore, an in situ FTIR study of methanol synthesis over Cu/ZnO concluded that adsorbed CO* species are necessary for the reduction of $HCOO^*$ to CH_3O^*.[66] Examining the structure sensitivity of methanol synthesis and the effect of morphological changes in detail is beyond the scope of this work. Nevertheless, we did consider the effect of CO on the removal of H_2O via the WGS reaction and on chemistry via CO-assisted hydrogenation reactions of various surface intermediates through a formyl intermediate (HCO^*) playing the role of H-carrier (see reactions R39−R45 in Table 2).

The first step in the CO-assisted hydrogenation is the formation of adsorbed HCO^* from coadsorbed CO* and H*. HCO^* formation is endothermic (ΔE = 0.78 eV) and has a moderate activation barrier of E_a = 0.99 eV. This activation barrier is in the same range of values as the barriers for direct hydrogenation of some of the key surface intermediates (see Table 2). Not only is this barrier comparable to most of the other barriers in the reaction scheme, but HCO^* is also not very stable, and the expected surface concentration could be rather low. If instead of HCO^*, its isomer, a COH^* intermediate was considered as a hydrogenation agent, then the energetics for the reaction $CO^* + H^* \rightarrow COH^* + *$ become ΔE = 1.15 eV and E_a = 2.26 eV, which are worse than the respective numbers for HCO^* formation. Therefore, we studied seven hydrogenation steps and compared the direct and CO-assisted hydrogenation via the HCO^*

dx.doi.org/10.1021/cs200055d |*ACS Catal.* 2011, 1, 365–384

Table 4. Promotional Effect of CO on Several Hydrogenation Steps[a]

reaction	E_a (direct hyrodgenation)/eV	E_a (CO-assisted hydrogenation)/eV
$CO^* \rightarrow HCO^*$	0.99	
$O^* \rightarrow OH^*$	0.96	spontaneous
$OH^* \rightarrow H_2O^*$	1.18	0.30
$HCOO^* \rightarrow HCOOH^*$	0.91	0.60
$HCOO^* \rightarrow H_2CO_2^*$	1.59	0.80
$HCOOH^* \rightarrow CH_3O_2^*$	1.04	0.42
$CH_2O^* \rightarrow CH_3O^*$	0.24	spontaneous
$CH_3O^* \rightarrow CH_3OH^*$	1.17	0.38

[a] E_a represents the calculated activation energy barrier for direct hydrogenation (H* is used as the H source) and for CO-assisted hydrogenation (HCO* is used as the H source).

intermediate. As shown in Table 4, the barriers for CO-assisted hydrogenation are always lower than for direct hydrogenation. This indicates that a promotional effect of CO via CO-assisted hydrogenation steps is possible, but the availability of adsorbed HCO* on the surface may be the key factor. We note that adsorbed HCO* may also react with adsorbed H* to H_2CO^* (E_a = 0.47 eV) and ultimately form methanol through the direct CO hydrogenation route.

Microkinetic Model. *Experimental Data.* After having analyzed the methanol synthesis and WGS reaction using DFT on the Cu(111) surface, a microkinetic model was developed using the DFT results as a starting point for the model parameters. We were unable to find an extensive kinetic data set collected on the Cu(111) surface. Instead, we used the comprehensive kinetic data set published by Graaf et al.,[27,28] which has been used by other authors[13,14,23,25] to compare their models with rates collected under realistic conditions on an industrially used catalyst. The kinetic data was collected in a spinning basket reactor at pressures between 15 and 50 atm and temperatures between 483 and 547 K over a $Cu/ZnO/Al_2O_3$ catalyst with various $H_2/CO_2/CO$ feed compositions. As pointed out by Askgaard et al., some of the experimental data points show deviations between measured methanol exit mole fractions and theoretical exit mole fractions derived from a material balance of up to 100%.[25] These data points may not have been collected at steady state. In addition, Graaf et al. observed intraparticle diffusion limitations at temperatures above 518 K.[28] We used the same criteria as Askgaard et al. and neglected data points collected above 518 K and those that show a relative exit mole fraction error of more than 40%.[25] A CSTR model was employed to simulate the spinning basket reactor; the number of Cu sites used was 300 μmol(sites)/g(catalyst).[122]

Parameter Estimation and Model Optimization. First, we used a parametrization of the microkinetic model which was based on our DFT results for the Cu(111) facet. The sticking coefficients of all adsorption steps were assumed to be 1. Without any further adjustment to the DFT-derived parameters, the microkinetic model predicts methanol synthesis rates that are 6 orders of magnitude smaller than measured rates on the industrial catalyst. Both CO and CO_2 hydrogenation contribute to the overall methanol synthesis rate, along the pathways $CO^* \rightarrow HCO^* \rightarrow CH_2O^* \rightarrow CH_3O^* \rightarrow CH_3OH^*$ and $CO_2^* \rightarrow HCOO^* \rightarrow HCOOH^* \rightarrow CH_3O_2^* \rightarrow CH_2O^* \rightarrow CH_3O^* \rightarrow CH_3OH^*$. The reverse WGS reaction also proceeds through two routes: direct CO_2 dissociation to CO and indirect via the COOH* intermediate. Starting from a $CO/CO_2/H_2$ mixture, HCOOH and CH_3OH are the main products of the reaction. CH_2O desorption is also present to a smaller extent, but almost no $HCOOCH_3$ is formed. Since methanol synthesis typically has a high selectivity toward methanol production, it is clear that the DFT-derived parameters on the Cu(111) surface are not adequate to describe the reaction on a commercial catalyst under industrial conditions. Some parameter adjustments will be necessary to account for differences between the ideal Cu(111) surface and the realistic $Cu/ZnO/Al_2O_3$ catalyst.

The number of adjustable parameters in our complex model with 49 elementary steps is quite large, and multiple solutions could be found that fit the experimental data reasonably well. For the DFT parameter set, the methanol synthesis rate is most sensitive to the binding energies of HCO* and CH_2O^*. Stabilizing these two intermediates by 0.4−0.5 eV accelerates the CO hydrogenation pathway by 3−4 orders of magnitude, but the calculated H_2O formation rates remain 5 orders of magnitude too small. To balance the contributions from CO and CO_2, we took a two-step approach. First, we focused only on the WGS reaction and did a preliminary fit of the WGS-relevant parameter subset to the kinetic data set reported by Koryabkina et al. on $Cu/ZnO/Al_2O_3$.[123] The optimization was not fully converged and stopped as soon as the calculated WGS rate was in the same order of magnitude as the experimental rate. Since the WGS reaction acts as a link between the CO and CO_2 hydrogenation pathways, we believe that starting the full optimization for methanol synthesis with a preoptimized WGS model will give a better result for the relative contributions of the CO and CO_2 hydrogenation routes.

Next, for the full optimization of the methanol synthesis reaction, we identified the 31 parameters given in the left column of Table 5, which are most relevant for the three active reaction pathways when pure DFT numbers were used (i.e., CO hydrogenation, CO_2 hydrogenation, and WGS). Sticking coefficients were not fitted because we found no influence of sticking coefficients for values between 0.01 and 1.0 for all adsorption steps. Hence, adsorption and desorption steps can be assumed to be quasi-equilibrated. The final parameter values after performing a least-squares fit to the experimental data by Graaf et al.[27,28] are given in Table 5. The objective function of the fit was formulated to account for CH_3OH and H_2O production rates simultaneously and with equal weights for these two quantities. The parity plot of experimental and calculated rates for the production rates of CH_3OH and H_2O (see Figure 4) shows a good fit with an R^2 value of 0.90 for CH_3OH and 0.94 for H_2O rates (R^2 = 0.92 overall). After this parameter fitting, the 6-orders of magnitude gap in measured versus predicted rates is closed, the selectivity to CH_3OH is high, and the desorption of HCOOH, CH_2O, and $HCOOCH_3$ as byproducts is negligible. The decreased production of HCOOH and CH_2O as compared with the model with the DFT-derived parameters can be, at least in part, attributed to the significant increase in the stability of these surface species (∼−0.5 eV).

The absolute value of parameter ω is difficult to define on the basis of DFT calculations and was only approximated from the reaction coordinates of the transition and final states. The choice of initial and final state in an NEB calculation can significantly influence the reaction coordinates, and the estimate for ω can vary widely. Therefore, it is not possible to critically discuss any

Table 5. Fully Optimized Parameter Set Used in the Microkinetic Model[a]

parameter	optimized value
ΔH_{fit} (H)	−0.07 eV
ΔH_{fit} (O)	0.00 eV
ΔH_{fit} (OH)	−0.41 eV
ΔH_{fit} (H_2O)	0.00 eV
ΔH_{fit} (CO)	0.10 eV
ΔH_{fit} (CO_2)	0.00 eV
ΔH_{fit} (COOH)	−0.31 eV
ΔH_{fit} (HCO)	−0.55 eV
ΔH_{fit} (HCOO)	−0.60 eV
ΔH_{fit} (H_2COO)	0.00 eV
ΔH_{fit} (HCOOH)	−0. 49 eV
ΔH_{fit} (CH_3O_2)	−0.55 eV
ΔH_{fit} (CH_2O)	−0.43 eV
ΔH_{fit} (CH_3O)	−0.64 eV
ΔH_{fit} (CH_2OH)	0.00 eV
ΔH_{fit} (CH_3OH)	−0.23 eV
$\omega(CO^* + H^* \rightarrow HCO^* + *)$	0.68
$\omega(HCO^* + H^* \rightarrow CH_2O^* + *)$	0.26
$\omega(CH_2O^* + H^* \rightarrow CH_3O^* + *)$	0.21
$\omega(CO_2^* + H^* \rightarrow HCOO^* + *)$	0.82
$\omega(HCOO^* + H^* \rightarrow HCOOH^* + *)$	0.68
$\omega(HCOO^* + H^* \rightarrow H_2CO_2^* + *)$	0.33
$\omega(HCOOH^* + H^* \rightarrow CH_3O_2^*)$	0.30
$\omega(CO^* + O^* \rightarrow CO_2^* + *)$	0.23
$\omega(CO^* + OH^* \rightarrow COOH^* + *)$	0.59
$\omega(COOH^* + * \rightarrow CO_2^* + H^*)$	0.33
$\omega(H_2O^* + * \rightarrow OH^* + H^*)$	0.87
$\omega(OH^* + * \rightarrow O^* + H^*)$	0.91
$\omega(2\ OH^* + * \rightarrow H_2O^* + O^*)$	0.66
$\omega(COOH^* + H^* \rightarrow HCOOH^* + *)$	0.27
$\omega(CH_3O^* + H^* \rightarrow CH_3OH^* + *)$	0.60

[a] $\Delta H_{fit}(X)$ is the deviation of the fitted enthalpy of species X from the DFT value; that is, $\Delta H_{fit} = 0$ eV means no adjustment was necessary. A negative entry for $\Delta H_{fit}(X)$ means that species X was stabilized on the catalyst surface compared to the DFT-derived parameter for binding of species X on Cu(111). $\omega(R)$ is the proximity factor of the transition state of reaction R.

deviations between the DFT estimates and the fitted values for ω. The DFT estimates were merely used as initial guesses. However, BEs are well-defined, and any differences between DFT values and fitted parameters carry useful information. The biggest deviations are found for the BEs of the following intermediates: OH*, COOH*, HCO*, HCOO*, HCOOH*, CH_3O_2*, CH_2O*, CH_3O*, and CH_3OH*. In the case of H*, and CO* the difference is ∼0.1 eV and well within the error bars of our calculations. For all other species, a stabilization of 0.3−0.6 eV is necessary, which merits a more detailed discussion.

First, we note that all binding energies were calculated on a static surface, and although relaxation effects are expected to be small, they may contribute with a stabilization of 0.1−0.2 eV for strong, interacting, surface radical species, such as OH*, COOH*, HCO*, HCOO*, CH_3O_2*, and CH_3O*. In the case of the three closed-shell molecules (CH_2O*, HCOOH*, and CH_3OH*), all showing weak interactions with the Cu(111) surface, the

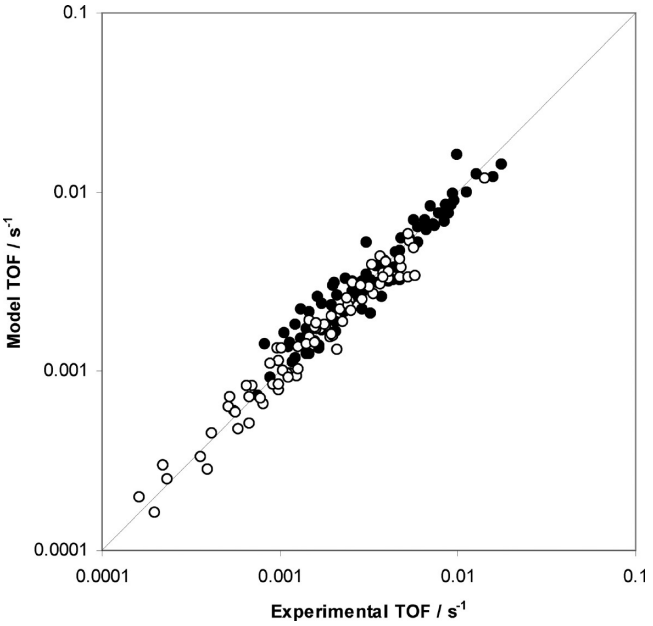

Figure 4. Parity plot of experimental and calculated TOF. Full circles represent CH_3OH production rates; open circles, H_2O production rates. Experimental data is taken from refs 27 and 28. Quality of fit: R^2-(CH_3OH) = 0.90, R^2 (H_2O) = 0.94, R^2 (overall) = 0.92.

difference may be caused by the deficiency of standard DFT methods to account for long-range interactions, such as van der Waals forces,[124] which may dominate the binding interactions for these stable molecules.

A theoretical method which is capable of describing van der Waals interactions[125] was recently presented. In the case of benzene adsorption on graphite, the additional energy contribution is ∼−0.5 eV. For transition metal surfaces, a good estimate for the van der Waals contributions is ∼0.1−0.2 eV per carbon atom, not enough to explain the additional stabilization needed in our microkinetic model for these three species. However, the fitted BE(CH_2O) = −0.49 eV agrees well with the measured heat of adsorption of CH_2O on Cu(110) of −0.59 eV, and similarly, the fitted BE(CH_3OH) = −0.51 eV is within the measured value of −0.72 eV for CH_3OH on oxidized Cu(110).[104] The deviations between calculated and fitted binding energies cannot be simply attributed to inaccuracies in our DFT methods, and the possibility of an active site different from the Cu(111) facet for methanol synthesis will be discussed later.

Reaction Mechanism. After fitting the microkinetic model to the experimental data, we can analyze the reaction mechanism and indentify key elementary steps in the model. A scheme including the most important reaction steps, according to the model fit, is given in Figure 5. Methanol is produced primarily from CO_2 hydrogenation through the following sequence of intermediates: HCOO*, HCOOH*, CH_3O_2*, CH_2O*, and CH_3O*. Methanol is also produced from CO hydrogenation through another sequence of intermediates: HCO*, CH_2O*, and CH_3O*. Pathways involving H_2CO_2* or CH_2OH* are not significant and can be neglected from the rest of the mechanistic analysis. Desorption of HCOOH and CH_2O is not observed after both surface species were stabilized during the fitting procedure by almost −0.5 eV with respect to the respective DFT binding energies. At typical conditions from the data set of Graaf et al.[27,28] (T = 499.3 K, P = 29.9 atm, y_{CO} = 0.053, y_{CO_2} =

dx.doi.org/10.1021/cs200055d |ACS Catal. 2011, 1, 365–384

0.047, $y_{H_2} = 0.90$), the surface is covered with 0.21 ML of CH_3O^*, 0.18 ML of H*, 0.04 ML of HCOO*, and 3×10^{-3} ML of OH*. No substantial coverage of atomic O* is found. Under these typical conditions, roughly 2/3 of CH_3OH is formed from CO_2, and the balance, from CO hydrogenation.

Calverley and Smith suggested that CO and CO_2 hydrogenation occurs independently on different types of active sites;[127] however, the degrees of rate control[126] obtained in our microkinetic model (Table 6) suggest that the relative contribution of both pathways is largely determined by the kinetics of the slow steps $HCO^* + H^* \rightarrow CH_2O^* + *$ and $HCOOH^* + H^* \rightarrow CH_3O_2 + *$. The hydrogenation of CH_3O^* to CH_3OH^* also has a high degree of rate control and is common to both routes for methanol production. HCO* primarily reacts to CH_2O^* and does not significantly participate in CO-assisted hydrogenation of other reaction intermediates. For CO_2-containing feeds, OH* is formed in the step $CH_3O_2^* + * \rightarrow CH_2O^* + OH^*$ (R23) and reacts mainly with H* to form H_2O^* (R14, ~48%), with CO* to COOH* (R10, ~26%), or with COOH* to $CO_2^* + H_2O^*$ (R12, ~26%). The last two OH* consumption steps represent the main pathway for the WGS reaction: $CO^* + 2\ OH^* \rightarrow COOH^* + OH^* + * \rightarrow CO_2^* + H_2O^* + *$. At least for the conditions represented by the values in Table 6, both steps show small degrees of rate control for CH_3OH production, indicating that methanol synthesis rates from $CO/CO_2/H_2$ mixtures show only a small sensitivity to the WGS activity of the catalyst. However, higher WGS activity promotes the consumption of CO and reduces the adsorption of CO_2, as seen by the positive degrees of rate control for CO adsorption and negative degrees of rate control for CO_2 adsorption.

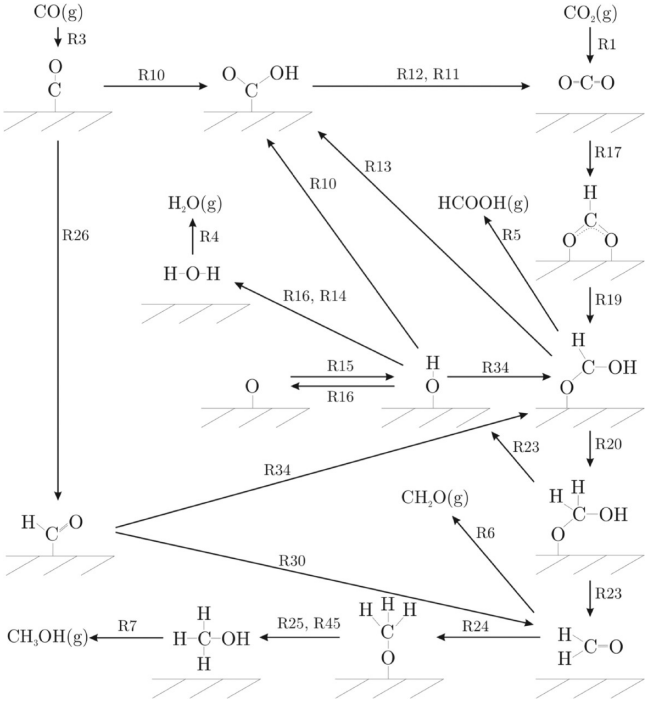

Figure 5. Reaction network of simultaneous methanol synthesis and WGS reaction over Cu catalysts. The labels R# refer to the reaction numbers provided in Table 2 and indicate the relevant steps to convert one main intermediate to the next one.

The importance of a comprehensive microkinetic model and the simultaneous investigation of CO/CO_2 hydrogenation and the WGS reaction becomes evident by looking at the PES in Figure 6. The PES shows reaction enthalpies and activation energy barriers after fitting of the microkinetic model to experimental methanol synthesis data for CO_2 hydrogenation (blue), CO hydrogenation (green), and the (reverse)WGS reaction (red). The hydrogenation of CH_2O^* to CH_3O^* and then to CH_3OH is a common path to all methanol formation routes and is given with the black line in Figure 6. A direct comparison between the CO hydrogenation pathway (state 2 → green line → black line → state 3) and the CO_2 hydrogenation pathway (state 1 → blue line → black line → state 3 → blue line → state 4) to CH_3OH would suggest that CO hydrogenation is the dominant reaction, because (i) it is more exothermic than CO_2 hydrogenation, (ii) the largest barrier is CH_3O^* hydrogenation (black line), which is also a part of the CO_2 pathway, and (iii) there exists a large barrier for OH* hydrogenation to form H_2O^* (blue line after state 3), which is a step involved in CO_2 hydrogenation to CH_3OH. Nevertheless, only ~1/3 of the produced methanol originates from CO.

The explanation for this nonintuitive result is that CO* is more efficiently consumed by a path competitive to its hydrogenation toward HCO*. In particular, CO* has to overcome only a small barrier to react with 2OH* to COOH* + OH* and eventually to $CO_2^* + H_2O^*$ (WGS). This reaction not only consumes CO but also facilitates the formation of H_2O, bypassing the highly activated $OH^* + H^* \rightarrow H_2O^* + *$ step. The promotional effect of CO on CO_2 hydrogenation is nicely illustrated in Figure 6: starting at state 3 and comparing the blue path to state 4 versus the red path to state 5 clearly shows the kinetic and thermodynamic preference to remove OH* with CO* via the WGS reaction. This explanation agrees well with the degrees of rate control we determined for the WGS and water dissociation steps in Table 6: higher WGS activity increases the adsorption of CO and is somewhat beneficial for CH_3OH production. In addition to the OH* hydrogenation barrier, other steps with high barriers in the CO_2 hydrogenation path are $HCOOH^* + H^* \rightarrow CH_3O_2^*$

Table 6. Degrees of Rate Control[126] for Adsorption and Desorption Reactions of CH_3OH, H_2, CO, CO_2, and H_2O[a]

	CH_3OH desorption	H_2 adsorption	CO adsorption	CO_2 adsorption	H_2O desorption
$H_2O^* + * \rightarrow OH^* + H^*$	0.00	0.01	−0.02	0.03	0.03
$OH^* + CO^* \rightarrow COOH^* + *$	0.01	0.00	0.09	−0.08	−0.08
$COOH^* + OH^* \rightarrow CO_2^* + H_2O^*$	0.01	0.00	0.04	−0.03	−0.03
$HCO^* + H^* \rightarrow CH_2O^* + *$	0.20	0.15	0.42	−0.08	−0.08
$HCOOH^* + H^* \rightarrow CH_3O_2^* + *$	0.22	0.25	0.09	0.38	0.38
$CH_3O_2^* + * \rightarrow CH_2O^* + OH^*$	0.00	0.00	0.00	0.01	0.01
$CH_3O^* + H^* \rightarrow CH_3OH^* + *$	0.20	0.19	0.24	0.15	0.15

[a] Values are reported for T = 499.3 K, P = 29.9 atm, $y_{CO} = 0.053$, $y_{CO_2} = 0.047$, $y_{H_2} = 0.90$ using a CSTR reactor model.

dx.doi.org/10.1021/cs200055d |ACS Catal. 2011, 1, 365–384

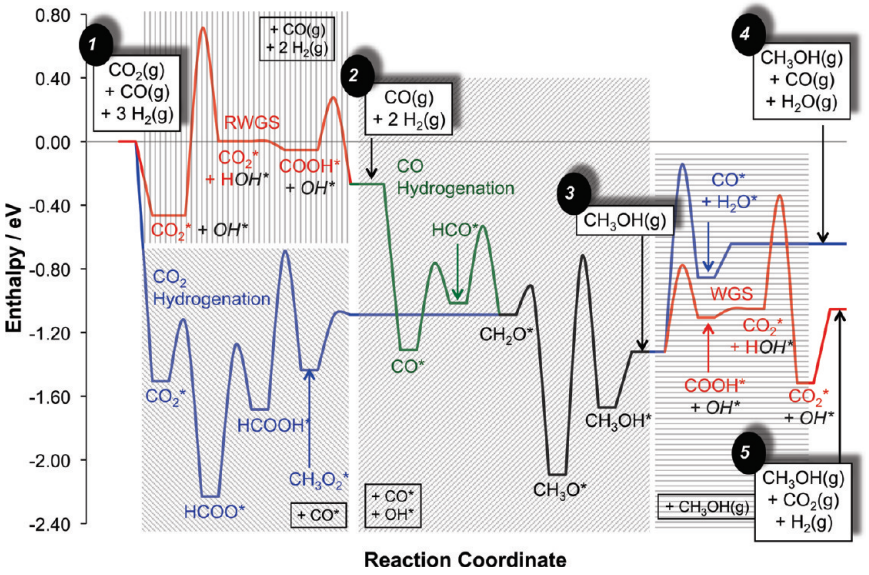

Figure 6. Potential energy surface for methanol synthesis reactions after fitting of the microkinetic model to experimental data. Enthalpies at 499 K are shown and referenced to CO_2(g) + CO(g) + 3 H_2(g). To improve readability, adsorbed H* atoms have been omitted from all labels, and spectator species along certain pathways are represented by black boxes in the shaded areas. For the (reverse) WGS reactions (red), we assume the presence of an additional OH*, marked with dark gray and italic font. The CO_2 hydrogenation with only spectator CO is given by the path: state 1 → blue line → black line → state 3 → blue line → state 4. CO_2 hydrogenation followed by WGS in the presence of CO proceeds along: state 1 → blue line → black line → state 3 → red line → state 5. CO hydrogenation takes place from state 2 to state 3 along the green → black path. The reverse WGS path starting from CO_2 and followed by CO hydrogenation goes from state 1 → red line → state 2 → green line → black line → state 3 → blue line → to state 4. Last, the WGS reaction is shown as the sequence: state 4 → blue line → state 3 → red line → state 5. The black path from CH_2O* to CH_3OH(g) is common to all CO and CO_2 hydrogenation routes.

+ * and CH_3O* hydrogenation, in good agreement with the degrees of rate control we found for these steps.

The WGS mechanism is in agreement with our earlier combined DFT and microkinetic modeling study, which found COOH* to be the key intermediate responsible for turning over WGS rates.[34] A COOH-type intermediate in the reverse WGS reaction has been proposed in the associative mechanism by Clarke and Bell derived from IR experiments and literature surveys.[110] The same authors also considered a HCOOH* complex during the hydrogenation of HCOO* to H_2CO_2*, which is similar to the HCOO* hydrogenation mechanism we propose. Indeed, introducing small amounts of HCOOH to the syngas feed increased the methanol yield for Cu/ZnO, Cu/ZrO_2, and Cu/MgO catalysts.[128] An intermediate with the same stoichiometry as HCOOH was also suggested in the forward and reverse WGS reaction and can be formed in the reaction of CO_2 and H_2.[64]

The first intermediate in the methanol synthesis reaction from CO_2 is HCOO*. Spectroscopic evidence for HCOO* on Cu catalysts is overwhelming, and there is no doubt that HCOO* is pivotal in the mechanism.[56] MS-IR and SSITKA studies have shown that the formation and decomposition of HCOO* from and into CO_2 and H_2 is very fast and quasi-equilibrated under methanol synthesis conditions on Cu/SiO_2.[129] Only on Cu/ZrO_2 was it reported that HCOO* is a spectator species and a precursor to methane formation, whereas methanol synthesis proceeds through CO hydrogenation after CO* is formed from CO_2 via a CO_3* intermediate.[98] We find that HCOO* is formed readily from CO_2 and adsorbed H* and that no CO_3* intermediate is necessary. Although our model does not include a mechanism for the formation of HCOO* from CO_3*, the rate of CO_3* formation in our model is small, and the CO_3* coverage is extremely low. This agrees well with experimental surface science studies on flat Cu surfaces.[90−93] CO_3* has been primarily observed on rough and stepped Cu surfaces[72,85] or strained surfaces with high defect concentrations.[130] These more complex surfaces were not considered in our DFT work; the thermochemistry and kinetics of various steps on these surfaces could be drastically different from those on Cu(111).[88] Hence, on the basis of this present work, we cannot exclude that on more open/rough surfaces, the CO_3* intermediate may play a role in methanol synthesis. CH_3O_2* is the key intermediate in the CO_2 hydrogenation mechanism proposed here. CH_3O_2* can be formed from HCOO* through HCOOH* with barriers that are smaller than the barrier for H_2CO_2* formation from HCOO*. The formation of CH_3O_2* from HCOOH* is a slow step in the CO_2 hydrogenation route, but after its formation, CH_3O_2* is easily converted into CH_2O* and OH*. In the CO hydrogenation pathway, CH_2O* is produced from CO* through hydrogenation of the HCO* intermediate. Hydrogenation of CH_2O* leads to CH_3O*, which is ultimately hydrogenated to CH_3OH*.

The mechanism we propose here suggests that the key intermediates for the WGS reaction and methanol synthesis are different. By application of various experimental techniques including IR, in situ FTIR, TPR and isotopic labeling, other authors have arrived at the same conclusion.[8,98,110,131] Accordingly, it should be possible to influence the selectivity between methanol synthesis and WGS by the addition of suitable promoters/inhibitors. In fact, it has been shown that adding potassium to Cu/SiO_2 enhances the reverse WGS reaction while hindering methanol synthesis.[110] Importantly, for industrial applications, Haldor Topsøe offers a commercial Cs-promoted low-temperature WGS catalyst capable of suppressing the undesired production of CH_3OH (LK-823).[132]

dx.doi.org/10.1021/cs200055d |*ACS Catal.* 2011, 1, 365–384

The Active Site for Methanol Synthesis. The fact that many intermediates needed to be stabilized by a similar amount to fit the experimental data set indicates a rather systematic error; that is, the Cu(111) facet may not be the most accurate representation of the active site for methanol synthesis. In addition, the structure sensitivity of methanol synthesis has been demonstrated through activity measurements on Cu(110), Cu(100), and polycrystalline Cu, where Cu(110) showed the highest turnover frequency.[15,16] All DFT calculations in this work were performed on the Cu(111) facet, which is thermodynamically the most stable but less reactive than more open facets (e.g., Cu(110), Cu(100)) or even step and defect sites. In a recent DFT study on CH_3OH oxidation, the binding energies of several intermediates on Cu(110) were published.[108] The biggest effect of the different surface structure is seen for CH_3O^*, $H_2CO_2^*$, and $HCOO^*$. These adsorbates show an increased magnitude of the BE, as compared with our values on Cu(111), by 0.49, 0.85, and 0.69 eV, respectively. It is well-known that step sites play a crucial role in syngas catalysis,[133] and the stability gain on the stepped Cu(211) versus the Cu(111) surface was estimated as −0.4 eV for OH^*, −0.3 eV for HCO^*, −0.3 eV for $H_2CO_2^*$, −0.2 eV for $HCOOH^*$, −0.3 eV for $CH_3O_2^*$, −0.2 eV for CH_2O^*, −0.4 eV for CH_3O^*, and −0.2 eV for CH_3OH^*.[134] For kink or defect sites, an even larger stabilization of the intermediates is expected.

Our DFT studies of various coadsorbed species on Cu(111) have shown that O^* and OH^* exhibit attractive interactions with many other intermediates. The attraction was usually in the range of −0.1 to −0.2 eV, but it is to be expected that the attractive interactions depend on surface coverages. In turn, O^*/OH^* coverage will depend strongly on the reaction conditions, especially the reduction/oxidation potential of the gas phase. For CO-rich feeds (strongly reducing conditions), we expect a negligible O^*/OH^* coverage, whereas some O^* and OH^* is expected for more oxidizing conditions (CO_2 or H_2O in the feed). Sakong and Gross investigated CH_3OH adsorption on the O-covered Cu(110) surface and found that the BE of CH_3OH varies between −0.05 and −0.77 eV.[108] The strongest BE of −0.77 eV corresponds to CH_3OH adsorption at the end of a CuO chain.

In summary, a comparison between the microkinetic model fitted BEs and the DFT values on the Cu(111) surface suggests that partially O^*/OH^*-covered step/defect sites may be a more suitable representation of the active site for methanol synthesis. Although the arguments we present here (stabilization by surface oxygen and structure sensitivity) may seem sufficient to explain the difference between the fitted BEs and the DFT values on Cu(111), our results cannot exclude support effects through Cu-support interactions,[7,135] reaction at the Cu-support interface,[107] or adsorption of species onto the support itself.[19,20]

The Role of CO. The effect of CO in methanol synthesis from $CO/CO_2/H_2$ mixtures is mostly thought to be negligible or strictly promotional.[9,10,102,136] In contrast, very early studies by Natta[6] and the Klier group[7] proposed that the CO-to-CH_3OH route is dominant. It has also been reported that the methanol synthesis rate increases by ∼70% with CO partial pressure over Cu(110).[15] Our results show that the effect of CO is not only promotional, but that both CO and CO_2 are hydrogenated and ultimately produce CH_3OH.

Simultaneous CH_3OH production from CO and CO_2 hydrogenation has been proposed in other theoretical[107,127] and experimental[27,137] studies. With our model, we tested two possibilities for a purely promotional effect of CO. First, CO removes OH^*/H_2O^*, which is formed during CO_2 hydrogenation, via the WGS reaction and shifts the reaction equilibrium toward CO_2 and H_2. Second, CO can facilitate the hydrogenation of other CO_2 hydrogenation intermediates via the formation of HCO^*. Our microkinetic model simulations suggest that only the former promotional pathway (via the WGS reaction) shows a significant contribution. Under the same conditions as above (T = 499.3 K, P = 29.9 atm, y_{CO} = 0.053, y_{CO_2} = 0.047, y_{H_2} = 0.90), the rate of the WGS reaction via $COOH^*$ is ∼16% of the rate of CH_3OH production. CO is consumed to 28% by the WGS reaction and to 72% by CO hydrogenation to CH_2O. Our model does not allow testing for the possibility of CO promotion by surface reconstructions induced by changes in the CO gas phase reduction potential, but the importance of this effect should not be neglected.[22,23]

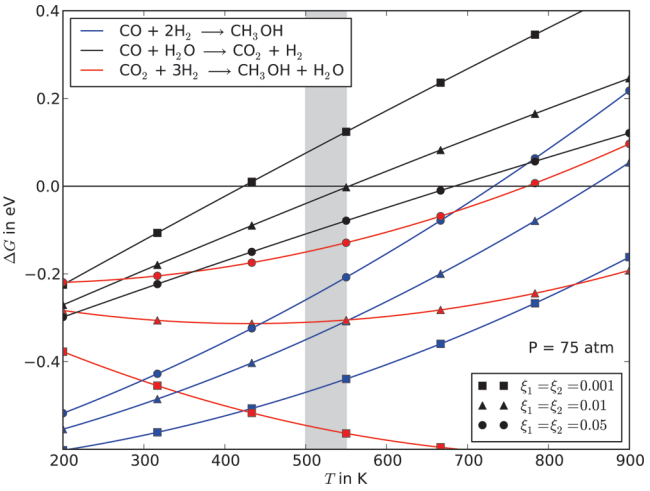

Figure 7. Gibb's free energy change, ΔG, for CO and CO_2 hydrogenation to CH_3OH and the WGS reaction at P = 75 atm and three different conversion levels as a function of temperature. ΔG is calculated using tabulated energy and entropy values and assuming ideal gas behavior. The overall gas phase composition is obtained from a feed composition of $CO/CO_2/H_2$ = 10/10/80 and equal extents of reaction ξ_1 for $CO + 2H_2 \rightarrow CH_3OH$ and ξ_2 for $CO_2 + 3H_2 \rightarrow CH_3OH + H_2O$. $\xi_1 = \xi_2$ = 0.1 corresponds to complete conversion of all available CO and CO_2 to CH_3OH. The shaded area represents the typical range of temperature for industrial methanol synthesis.

Methanol Synthesis Dependence on CO/CO_2 feed Ratio at Industrial Conditions. Among the most powerful features of a microkinetic model is its ability to predict reaction rates at various temperature, pressure, and feed composition conditions. This can be very useful for both the improved understanding of the reaction mechanism and for practical applications, such as chemical reactor design.[47] Before we discuss the kinetic aspects of methanol synthesis, it is instructive to look at the overall thermodynamics of the simultaneously occurring reactions. Typically, methanol synthesis is carried out at 523 K, P = 50−100 atm and feed compositions of $CO/CO_2/H_2$ = 10/10/80.[9]

In Figure 7, we show the Gibb's free energy change of CO and CO_2 hydrogenation to CH_3OH as well as that of the WGS reaction as a function of temperature at P = 75 atm. The gray shaded area indicates the typical temperature range. The more negative the ΔG for a reaction, the higher its thermodynamic driving force. Initially, at very low conversions (squares), CO_2 hydrogenation has the highest thermodynamic driving force in the temperature range of interest. The WGS reaction proceeds in

dx.doi.org/10.1021/cs200055d |*ACS Catal.* 2011, 1, 365–384

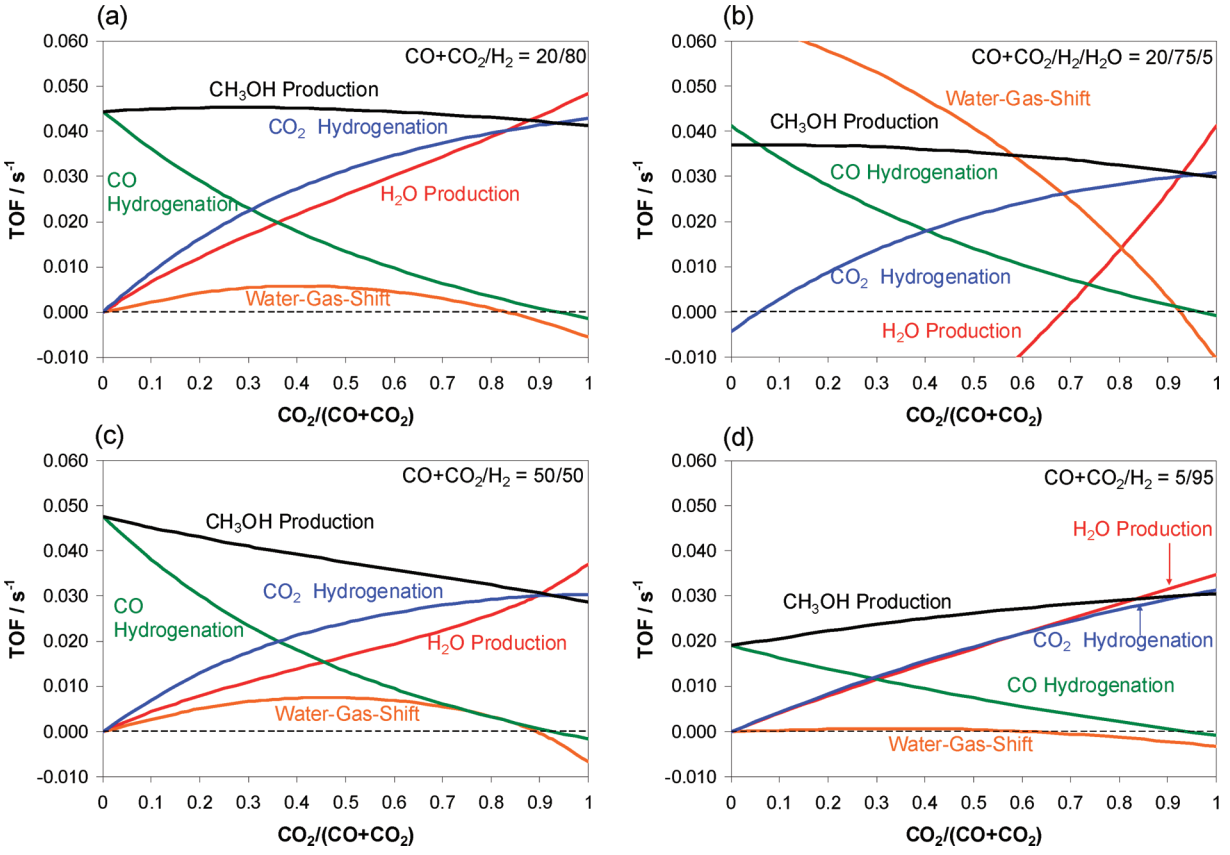

Figure 8. Calculated turnover frequencies (TOF) as a function of $CO_2/(CO + CO_2)$ ratio and different feed compositions at $P = 75$ atm, $T = 528$ K: (a) $(CO + CO_2)/H_2 = 20/80$, (b) $(CO + CO_2)/H_2/H_2O = 20/75/5$, (c) $(CO + CO_2)/H_2 = 50/50$, and (d) $(CO + CO_2)/H_2 = 5/95$.

the reverse direction (positive ΔG) and converts some CO_2 to CO. At ~10% conversion of CO and CO_2 ($\xi_1 = \xi_2 = 0.01$, triangles), both routes have the same driving force and the WGS reaction is equilibrated. At higher conversions (circles), CO hydrogenation has the most negative ΔG, and the WGS reaction runs in the forward direction. Although this analysis is based purely on the overall thermodynamics, it clearly shows that the reaction conditions and conversion levels can have a significant influence on the driving forces for competing CO and CO_2 hydrogenation and may even reverse the direction of the WGS reaction. Therefore, one must use caution with the interpretation of experimental data, and it may be inappropriate to extrapolate results regarding the relative importance of CO versus CO_2 hydrogenation from low temperature/pressure/conversion laboratory experiments to high temperature/pressure/conversion industrial conditions. In other words, conclusions about the main carbon source in CH_3OH can only be made for specific conditions and may not be generalized.

Next, we use our microkinetic model for exploring methanol synthesis kinetics at industrially relevant conditions ($T = 528$ K, $P = 75$ atm, $CO + CO_2/H_2 = 20/80$). Figure 8a shows simulated reaction rates of CO hydrogenation, CO_2 hydrogenation, WGS reaction, and the overall CH_3OH and H_2O production as a function of the $CO_2/(CO + CO_2)$ ratio. For pure CO/H_2 mixtures, methanol is exclusively produced from CO hydrogenation, and all other rates are zero. In the other extreme case of a binary CO_2/H_2 mixture, methanol is produced only from CO_2 hydrogenation, with the formation of H_2O as byproduct. For the binary CO_2/H_2 mixture, additional H_2O and CO are produced through the reverse WGS reaction ($CO_2 + H_2 \rightarrow CO + H_2O$) via the COOH intermediate, but we also observe a small contribution to reverse WGS via CH_2O, the first common intermediate of the CO and CO_2 hydrogenation route to CH_3OH, causing the negative CO hydrogenation rates for large $CO_2/(CO + CO_2)$ ratios in Figure 8. Both binary mixtures show a similar activity toward methanol production, but a shallow maximum exists for $CO_2/(CO + CO_2) \approx 0.3-0.5$, which is close to the typical ratio used for industrial purposes (0.5). In the range from $0.3 < CO_2/(CO + CO_2) < 1.0$, the larger fraction of methanol results from CO_2 hydrogenation. The surface coverages of CH_3O^*, $HCOO^*$, H^*, and OH^*, the only four species calculated to exist in observable quantities on the surface, are shown in Figure 9a. CH_3O^* is the most abundant surface species throughout these conditions. The coverage of $HCOO^*$ and OH^* increases with increasing CO_2 in the feed, consistent with the fact that these species participate only in the hydrogenation of CO_2.

In Figures 8b and 9b, we examine the effect of small amounts of water in the feed. When 5% water is included in the feed, the overall methanol production decreases, especially for CO_2-rich feeds, which is expected, since H_2O is a byproduct of CO_2 hydrogenation. The forward WGS rate increases dramatically, particularly at the CO-rich end of the feed composition spectrum, and some CH_2O^* originating from CO decomposes to CO_2, causing a negative CO_2 hydrogenation rate. The surface is covered with 5−10% less CH_3O^*, and the OH^* coverage increases to 1−3%.

We also investigated the effect of H_2 content in the feed and find a strong effect for CO-rich feeds. When the reaction is

dx.doi.org/10.1021/cs200055d |ACS Catal. 2011, 1, 365–384

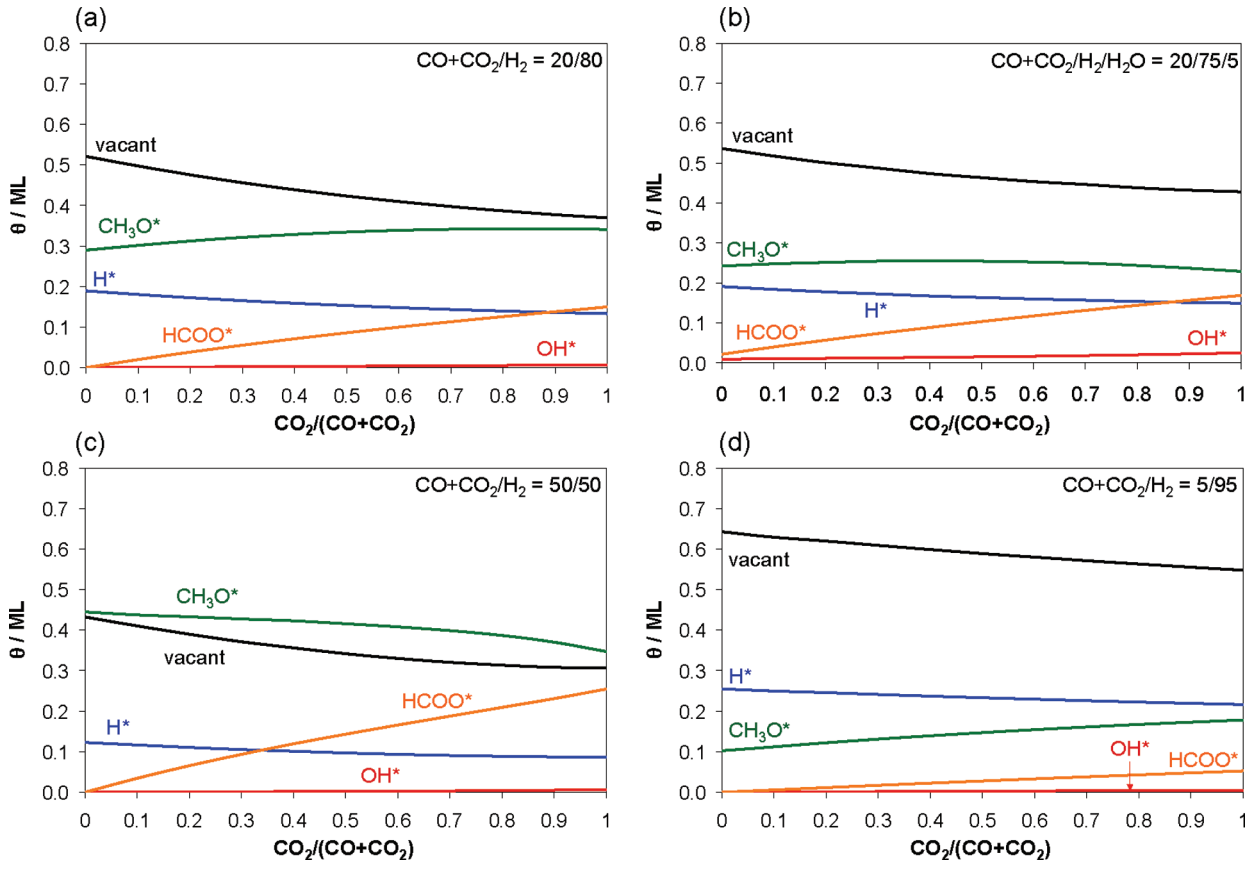

Figure 9. Surface coverage, θ, of the most abundant surface intermediates as a function of $CO_2/(CO + CO_2)$ ratio and different feed compositions at $P = 75$ atm, $T = 528$ K: (a) $(CO + CO_2)/H_2 = 20/80$, (b) $(CO + CO_2)/H_2/H_2O = 20/75/5$, (c) $(CO + CO_2)/H_2 = 50/50$, and (d) $(CO + CO_2)/H_2 = 5/95$.

running under lean hydrogen conditions (50% H_2, Figures 8c, 9c), the CO hydrogenation activity is slightly increased, and the overall methanol production decreases nearly linearly with increasing CO_2 content. In contrast, if there is excess hydrogen available (95% H_2, Figures 8d, 9d), the CO hydrogenation activity is low, and the overall methanol production increases with increasing CO_2 content. We can rationalize the different behavior under lean and rich hydrogen conditions by the hydrogen requirements of CO and CO_2 hydrogenation. The hydrogenation of 1 mol CO_2 to CH_3OH requires 3 mol of hydrogen, whereas the hydrogenation of 1 mol CO to CH_3OH requires only 2 mol of hydrogen. The contributions of CO and CO_2 hydrogenation to the overall CH_3OH production rate also depend on the total pressure (not shown): at low pressures, the relative contribution from CO_2 hydrogenation is larger than for high pressures and vice versa. This observation can be explained by invoking the Le Chatelier principle. In the CO hydrogenation pathway, 3 mol of reactants are converted to 1 mol of product (compression of 1/3), whereas in the CO_2 hydrogenation pathway, 4 mol are converted to 2 mol of product (compression of 1/2).

The majority of our observations under various conditions can be explained by looking at the surface coverages of CH_3O^* and H^*. We have previously identified step R25 ($CH_3O^* + H^* \rightarrow CH_3OH^* + *$) as the common slow step of both CH_3OH formation routes, and its forward rate depends linearly on the product $\theta_{CH_3O} \times \theta_H$. Figure 10a shows a comparison of the coverage product $\theta_{CH_3O} \times \theta_H$ (symbols) with the overall CH_3OH production rates (solid lines) for the four different conditions used in Figures 8 and 9. With the exception of the shallow maximum in our standard feed composition ($(CO + CO_2)/H_2 = 20/80$), all trends are qualitatively reproduced, and high methanol production rates are achieved for high simultaneous coverages of CH_3O^* and H^*.

To explain the maximum for the $(CO + CO_2)/H_2 = 20/80$ mixture, we take a closer look at the forward reaction rates of the key reactions, as shown in Figure 10b. The slow steps during CO and CO_2 hydrogenation to CH_3O^* are $HCO^* + H^* \rightarrow CH_2O^* + *$ (R30) and $HCOOH^* + H^* \rightarrow CH_3O_2^* + *$ (R20), respectively. By neglecting the reverse rates of R30 and R20 and taking the sum of the forward rates, we can find the upper limit of the achievable CH_3O^* formation rate via CO and CO_2 hydrogenation. The CH_3O^* formation rate increases with CO_2 content. On the other hand, the forward rate of CH_3O^* hydrogenation (R25) represents the fastest possible CH_3O^* consumption rate and decreases with CO_2 content, caused by the change of $\theta_{CH_3O} \times \theta_H$, as shown in Figure 10a. The maximal achievable CH_3O^* production and consumption rates form a volcano-shaped curve, whose top coincides approximately with the maximum of actual CH_3OH production. For low $CO_2/(CO + CO_2)$ ratios, the formation of CH_3O^* is limiting the production of CH_3OH, whereas at high $CO_2/(CO + CO_2)$ ratios, the CH_3O^* hydrogenation is rate-limiting. This analysis also indicates that in the binary CO/H_2 mixture, $HCO^* + H^* \rightarrow CH_2O^* + *$ is the slow step, and adding CO_2 to the reaction mixture opens a parallel pathway for CH_3O^* production with higher activity.

Several groups have experimentally studied the dependence of methanol synthesis rates on the CO/CO_2 feed ratio on various

dx.doi.org/10.1021/cs200055d |ACS Catal. 2011, 1, 365–384

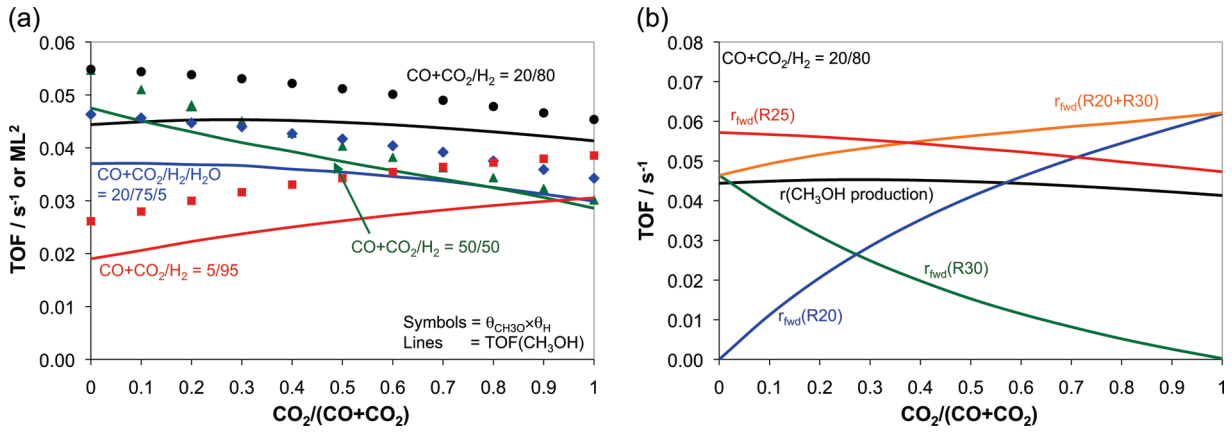

Figure 10. (a) Calculated methanol production rates (solid lines) for the four conditions in Figures 8 and 9 (P = 75 atm, T = 528 K). The symbols represent the product of the respective calculated surface coverages for CH_3O^* and H^* ($\theta_{CH_3O} \times \theta_H$). (b) Forward reaction rates of $HCO^* + H^* \rightarrow CH_2O^* + *$ (R30), $HCOOH^* + H^* \rightarrow CH_3O_2^* + *$ (R20), $CH_3O^* + H^* \rightarrow CH_3OH^* + *$ (R25), the sum of R20 + R30, and the overall CH_3OH production rate as a function of feed composition at P = 75 atm and T = 528 K. (Note: there is no common color code between the two panels.)

Table 7. Calculated Reaction Orders for CH_3OH Synthesis over Cu Catalysts at P = 75 atm and T = 528 K, for Four Different Feed Compositions

	CH_3OH from CO				CH_3OH from CO_2				CH_3OH overall			
feed composition $CO/CO_2/H_2/H_2O$	CO	CO_2	H_2	H_2O	CO	CO_2	H_2	H_2O	CO	CO_2	H_2	H_2O
10/0/80/0									0.73		0.68	
0/10/80/0										0.39	0.99	
10/10/80/0	1.34	−0.30	0.38		−0.07	0.73	0.88		0.08	0.15	0.72	
10/10/75/5	1.13	−0.21	0.31	0.02	−0.04	1.00	1.48	−0.13	0.16	0.16	0.99	−0.08

Cu-based catalysts. For example, Liu et al. reported a linear increase in CH_3OH production rate with increasing CO_2 content ($(CO + CO_2)/H_2$ = 30/70) on a Cu/ZnO catalyst (30% Cu, 70% Zn) at 17 atm and temperatures between 468 and 498 K.[138] The highest CH_3OH production rates were measured for the binary mixture of CO_2/H_2; even small amounts of H_2O, as little as 0.554%, had a strong negative effect on the production rate. Since we used a higher pressure and temperature (75 atm, 528 K) and different feed compositions, we cannot directly compare our model with the results of Liu et al., but the negative effect of H_2O is clearly reproduced (Figures 8b and 10a).

The linear increase in CH_3OH production rate with increasing CO_2 content observed by Liu et al. is reproduced by our model only for feeds with a high H_2 content (95%, Figure 8d). However, we mentioned above that lower pressures favor CO_2 hydrogenation, and it may require less H_2 at low pressures to observe the linear increase with CO_2 content. Fisher et al. measured the activation barriers for CH_3OH formation from CO and CO_2 on several unpromoted and ZrO_2-promoted Cu/SiO_2 catalysts and found lower activation barriers for CO_2 hydrogenation than for CO hydrogenation on all catalysts.[139] Consequently, the larger fraction of CH_3OH in $CO/CO_2/H_2$-containing feeds should originate from CO_2, in agreement with the results of our model.

Bourzutschky et al. investigated a variety of Cu-containing catalysts ($(CO + CO_2)/H_2$ = 75/25, T = 573, P = 13.4 atm) and found that the activity of NaO_x/Cu powder and Cu/La_2O_3 are very high for CO/H_2 mixtures and drops sharply when CO_2 is added.[140] On the other hand, the activity of Cu/SiO_2 reaches a maximum at $CO_2/(CO + CO_2)$ = 0.8 and reaches zero when no CO_2 is present. The behavior reported on Cu/SiO_2 resembles the behavior of industrially used $Cu/ZnO/Al_2O_3$ catalysts more closely and is in qualitative agreement with our microkinetic model for CO_2-rich feeds. However, for CO-rich feeds, our model predicts a significant activity, which was not observed by Bourzutschky et al. on Cu/SiO_2. No activity for CO/H_2 mixtures at T = 543 K and P = 1.4 bar was found by Nerlov et al. on Cu(100), and the CH_3OH production rate depends only on the partial pressures of CO_2.[136] The kinetic model and experimental results by Calverly and Smith suggest that $Cu/ZnO/Cr_2O_3$ catalysts show some activity for CO/H_2 mixtures, which drastically increases when small amounts of CO_2 are added.[127] The maximum CH_3OH production at 50 atm is found for CO-rich feeds with $0.05 < CO_2/(CO + CO_2) < 0.2$.

Although our model qualitatively captures and reproduces many experimental observations on different Cu-based catalysts, such as the high contributions of CO_2 hydrogenation and the existence of a maximum for certain feed compositions, there evidently exists a discrepancy for CO-rich feeds. Specifically, the experimental data by Calverly and Smith suggest that CO_2 could have a promotional effect on CO hydrogenation in CO-rich feeds. We note that our focus lies on CH_3OH production from CO_2 and the data set by Graaf et al.,[27,28] on which we based our parameter estimation, does not contain data for a pure binary CO/H_2 feed. Hence, for low $CO_2/(CO + CO_2)$ ratios, our predictions are mere extrapolations, and deviations in that range could be expected. However, one must also consider the possibility that a different mechanism may be dominating for CO-rich feeds or that the strong reducing potential of pure binary CO/H_2 mixtures changes the Cu particle shape,[22] which in turn affects the stability and reactivity of the main surface intermediates. Therefore, our fitted thermodynamic and kinetic parameters may not be representative under strongly reducing conditions.

dx.doi.org/10.1021/cs200055d |ACS Catal. 2011, 1, 365–384

Last, we briefly comment on the reaction orders of methanol synthesis. The calculated reaction orders should be used with caution because they strongly depend on feed composition and reaction conditions. Here, we chose four different feed compositions representing a typical mixed feed with $CO/CO_2/H_2$, the two binary mixtures of CO/H_2 and CO_2/H_2 (see Table 7), and a quaternary feed with H_2O, all at $P = 75$ atm and $T = 528$ K. In the ternary feed mixture (10/10/80), we find that the overall reaction order with respect to CO_2 (0.15) is larger than the reaction order with respect to CO (0.08), in qualitative agreement with our previous analysis showing that the larger fraction of CH_3OH is formed from CO_2. Increasing the pressure of CO (CO_2) increases the fraction of CH_3OH formed from CO (CO_2), as indicated by the reaction order of 1.34 (0.73); simultaneously, the contribution of CO_2 (CO) hydrogenation to CH_3OH production is reduced, as seen by the negative reaction order of −0.30 (−0.07). Further, we note that the larger reaction order with respect to H_2 for CH_3OH production from CO_2 (0.88) than from CO (0.38) is in excellent agreement with our findings that higher H_2 pressures favor CO_2 hydrogenation. The presence of small amounts of water in the feed has an adverse effect on the overall CH_3OH production (−0.08), which is largely caused by inhibition of the CO_2 hydrogenation pathway (−0.13). CH_3OH formation from CO, on the other hand, is slightly enhanced (0.02) by the presence of H_2O in the feed.

CONCLUSIONS

We performed an extensive set of periodic, self-consistent DFT calculations to determine the energetics of 22 surface species as well as the activation energy barriers and pre-exponential factors necessary to describe 49 elementary surface reactions on Cu(111), a representative stable facet of methanol synthesis catalytic nanoparticles. In addition to species that are part of previously suggested mechanisms, we also considered intermediates such as HCOOH* and CH_3O_2* and allowed for the formation of CH_2O, HCOOH, and $HCOOCH_3$ as byproducts. The DFT results show that hydrogenation of HCOO* preferentially leads to the formation of HCOOH*, not H_2CO_2*, which had been suggested previously. HCOOH* is then further hydrogenated to CH_3O_2*, which subsequently forms CH_2O* by splitting off its OH group. CH_3O* is the final intermediate before CH_3OH* is formed.

Guided by our detailed DFT results, a mean-field microkinetic model was fitted to published experimental methanol synthesis rate data, which were collected under realistic conditions on a commercial $Cu/ZnO/Al_2O_3$ catalyst. The model shows a good fit to the experimental data with $R^2 = 0.92$. Both CO and CO_2 hydrogenation pathways are active under typical methanol synthesis conditions, and the effect of CO is not only promotional. CO_2 is hydrogenated via the sequence CO_2* → HCOO* → HCOOH* → CH_3O_2* → CH_2O* → CH_3O* → CH_3OH*. The formation of HCOO* from CO_2* and adsorbed H* is fast and does not require a CO_3* intermediate. CO hydrogenation yields methanol through the sequence CO* → HCO* → CH_2O* → CH_3O* → CH_3OH*. The hydrogenation of CH_3O* is slow, and the product of CH_3O* and H* coverage ($\theta_{CH_3O} \times \theta_H$) qualitatively describes the behavior of overall methanol synthesis rates for a large range of conditions and CO_2-rich feed compositions. However, under some conditions, especially for CO-rich feeds, the formation of CH_3O* can be rate-limiting, resulting in a volcano-shaped curve for methanol production as a function of the $CO_2/(CO + CO_2)$ feed ratio. The relative contributions of CO and CO_2 hydrogenation pathways are determined by the steps HCO* + H* → CH_2O* + * in the CO route and HCOOH* + H* → CH_3O_2* + * in the CO_2 route and also depend on the reaction conditions. Under typical industrial conditions, 2/3 of the methanol is produced from CO_2 hydrogenation. Naturally, because the experimental data points used to fit our model were heavily probing CO_2-rich feeds, our microkinetic model performs well for CO_2-rich feed compositions, which are most relevant for CO_2 chemical fixation, but some discrepancies with other experimental observations for CO-rich feed compositions exist. The latter might be caused by an adsorbate (CO)-induced surface reconstruction when moving from oxidizing (CO_2-rich) to reducing (CO-rich) conditions, which, in turn, could affect the dominant reaction mechanism. We considered two possibilities that could explain the CO promotion of CO_2 hydrogenation: (a) removal of OH* via the WGS reaction and (b) CO-assisted hydrogenation via the HCO* intermediate. No evidence was found for the latter CO-promotion mechanism, but the removal of adsorbed OH* with CO* via the WGS reaction shows a considerable contribution to the reaction mechanism.

A comparison between binding energies calculated with DFT on the Cu(111) surface and the parameters obtained from fitting the microkinetic model suggests that the clean Cu(111) surface may not provide the most accurate representation of the active site on a commercial $Cu/ZnO/Al_2O_3$ catalyst. However, the fitted parameter values suggest that a more open and partially oxidized Cu facet (e.g., Cu(110), Cu(100), Cu(211)) might be a more suitable representation of the active site for methanol synthesis. Although it seems likely that only the Cu particles are responsible for the catalytic activity of the real catalyst, our work cannot exclude synergistic effects with the ZnO support. For more quantitative conclusions about the structure sensitivity of the reaction and the oxidation state of the surface, further studies would be needed.

ASSOCIATED CONTENT

Supporting Information. Gas phase corrections, entropy calculations, Shomate parameters, and transition state weights. This material is available free of charge via the Internet at http://pubs.acs.org.

AUTHOR INFORMATION

Corresponding Author
*Phone/Fax: (608) 262-9053. E-mail: manos@engr.wisc.edu.

ACKNOWLEDGMENT

Financial support for this work was provided in part by DOE/BES and by a Laboratory Directed Research and Development (LDRD) program at Sandia National Laboratories, LDRD 113486. Sandia is a multiprogram laboratory operated by Sandia Corporation, a Lockheed Martin Company, for the United States Department of Energy under Contract No. DE-AC04-94AL85000. The computational work was performed in part using supercomputing resources from the following institutions: EMSL, a National scientific user facility at Pacific Northwest National Laboratory (PNNL); the Center for Nanoscale Materials at Argonne National Laboratory (ANL); the National Center

for Computational Sciences at Oak Ridge National Laboratory (ORNL); and the National Energy Research Scientific Computing Center (NERSC). EMSL is sponsored by the Department of Energy's Office of Biological and Environmental Research located at PNNL. CNM, NCCS, and ORNL are supported by the U.S. Department of Energy, Office of Science, under contracts DE-AC02-06CH11357, DEAC05-00OR22725, and DE-AC02-05CH11231, respectively. We thank Profs. Charlie T. Campbell and Ib Chorkendorff, and Dr. Peter Ferrin for useful discussions. We also thank Carrie Farberow and Patricia Rubert-Nason for carefully proofreading the manuscript.

REFERENCES

(1) Miller, J.; Allendorf, M.; Diver, R.; Evans, L.; Siegel, N.; Stuecker, J. *J. Mater. Sci.* **2008**, *43*, 4714.
(2) Lee, S. *Methanol Synthesis Technology*; CRC Press: Boca Raton, Fl, 1989.
(3) Tremblay, J. F. *Chem. Eng. News* **2008**, *86*, 13.
(4) Baiker, A. *Appl. Organomet. Chem.* **2000**, *14*, 751.
(5) Olah, G. A.; Goeppert, A.; Prakash, G. K. S. *Beyond Oil and Gas: The Methanol Economy*; Wiley-VCH Verlag GmbH & Co. KGaA: Weinheim, 2006.
(6) Natta, G. In *Catalysis*; Emmett, P. H., Ed.; Reinhold: New York, 1955, p 349.
(7) Klier, K. *Adv. Catal.* **1982**, *31*, 243.
(8) Chinchen, G. C.; Denny, P. J.; Parker, D. G.; Spencer, M. S.; Whan, D. A. *Appl. Catal.* **1987**, *30*, 333.
(9) Waugh, K. C. *Catal. Today* **1992**, *15*, 51.
(10) Hansen, J. B.; Nielsen, P. E. H. In *Handbook of Heterogeneous Catalysis*; Ertl, G., Knözinger, H., Schüth, F., Weitkamp, J., Eds.; Wiley-VCH Verlag GmbH & Co. KGaA: Weinheim, 2008.
(11) Szanyi, J.; Goodman, D. W. *Catal. Lett.* **1991**, *10*, 383.
(12) Chinchen, G. C.; Waugh, K. C.; Whan, D. A. *Appl. Catal.* **1986**, *25*, 101.
(13) Rasmussen, P. B.; Kazuta, M.; Chorkendorff, I. *Surf. Sci.* **1994**, *318*, 267.
(14) Rasmussen, P. B.; Holmblad, P. M.; Askgaard, T.; Ovesen, C. V.; Stoltze, P.; Nørskov, J. K.; Chorkendorff, I. *Catal. Lett.* **1994**, *26*, 373.
(15) Yoshihara, J.; Campbell, C. T. *J. Catal.* **1996**, *161*, 776.
(16) Yoshihara, J.; Parker, S. C.; Schafer, A.; Campbell, C. T. *Catal. Lett.* **1995**, *31*, 313.
(17) Fujitani, T.; Nakamura, I.; Uchijima, T.; Nakamura, J. *Surf. Sci.* **1997**, *383*, 285.
(18) Fujitani, T.; Nakamura, I.; Watanabe, T.; Uchijima, T.; Nakamura, J. *Catal. Lett.* **1995**, *35*, 297.
(19) Burch, R.; Chappell, R. J.; Golunski, S. E. *J. Chem. Soc., Faraday Trans. I* **1989**, *85*, 3569.
(20) Joo, O. S.; Jung, K. D.; Han, S. H.; Uhm, S. J.; Lee, D. K.; Ihm, S. K. *Appl. Catal., A* **1996**, *135*, 273.
(21) Frost, J. C. *Nature* **1988**, *334*, 577.
(22) Hansen, P. L.; Wagner, J. B.; Helveg, S.; Rostrup-Nielsen, J. R.; Clausen, B. S.; Topsøe, H. *Science* **2002**, *295*, 2053.
(23) Ovesen, C. V.; Clausen, B. S.; Schiotz, J.; Stoltze, P.; Topsøe, H.; Nørskov, J. K. *J. Catal.* **1997**, *168*, 133.
(24) Creemer, J. F.; Helveg, S.; Hoveling, G. H.; Ullmann, S.; Molenbroek, A. M.; Sarro, P. M.; Zandbergen, H. W. *Ultramicroscopy* **2008**, *108*, 993.
(25) Askgaard, T. S.; Nørskov, J. K.; Ovesen, C. V.; Stoltze, P. *J. Catal.* **1995**, *156*, 229.
(26) VandenBussche, K. M.; Froment, G. F. *J. Catal.* **1996**, *161*, 1.
(27) Graaf, G. H.; Stamhuis, E. J.; Beenackers, A. A. C. M. *Chem. Eng. Sci.* **1988**, *43*, 3185.
(28) Graaf, G. H. Ph.D. Thesis, Rijksuniversiteit, Groningen, 1988.
(29) Taylor, P. A.; Rasmussen, P. B.; Chorkendorff, I. *J. Chem. Soc., Faraday Trans.* **1995**, *91*, 1267.
(30) Cramer, C. J.; Truhlar, D. G. *Phys. Chem. Chem. Phys.* **2009**, *11*, 10757.
(31) Nørskov, J. K.; Bligaard, T.; Rossmeisl, J.; Christensen, C. H. *Nature Chem.* **2009**, *1*, 37.
(32) Hammer, B.; Hansen, L. B.; Nørskov, J. K. *Phys. Rev. B* **1999**, *59*, 7413.
(33) Greeley, J.; Nørskov, J. K.; Mavrikakis, M. *Annu. Rev. Phys. Chem.* **2002**, *53*, 319.
(34) Gokhale, A. A.; Dumesic, J. A.; Mavrikakis, M. *J. Am. Chem. Soc.* **2008**, *130*, 1402.
(35) Ferrin, P.; Mavrikakis, M. *J. Am. Chem. Soc.* **2009**, *131*, 14381.
(36) Ferrin, P.; Nilekar, A. U.; Greeley, J.; Mavrikakis, M.; Rossmeisl, J. *Surf. Sci.* **2008**, *602*, 3424.
(37) Neugebauer, J.; Scheffler, M. *Phys. Rev. B* **1992**, *46*, 16067.
(38) Bengtsson, L. *Phys. Rev. B* **1999**, *59*, 12301.
(39) Vanderbilt, D. *Phys. Rev. B* **1990**, *41*, 7892.
(40) Perdew, J. P.; Chevary, J. A.; Vosko, S. H.; Jackson, K. A.; Pederson, M. R.; Singh, D. J.; Fiolhais, C. *Phys. Rev. B* **1992**, *46*, 6671.
(41) White, J. A.; Bird, D. M. *Phys. Rev. B* **1994**, *50*, 4954.
(42) Kresse, G.; Furthmüller, J. *Comput. Mater. Sci.* **1996**, *6*, 15.
(43) *CRC Handbook of Chemistry and Physics*, 76th ed.; CRC Press: New York, 1996.
(44) Greeley, J.; Mavrikakis, M. *Surf. Sci.* **2003**, *540*, 215.
(45) Ochterski, J. W. 1999.
(46) Dumesic, J. A.; Rudd, D. F.; Aparicio, L. L.; Rekoske, J. E.; Treviño, A. A. *The Microkinetics of Heterogeneous Catalysis*; American Chemical Society: Washington, DC, 1993.
(47) Gokhale, A. A.; Kandoi, S.; Greeley, J. P.; Mavrikakis, M.; Dumesic, J. A. *Chem. Eng. Sci.* **2004**, *59*, 4679.
(48) Temel, B.; Meskine, H.; Reuter, K.; Scheffler, M.; Metiu, H. *J. Chem. Phys.* **2007**, *126*, 204711.
(49) Honkala, K.; Hellman, A.; Remediakis, I. N.; Logadottir, A.; Carlsson, A.; Dahl, S.; Christensen, C. H.; Nørskov, J. K. *Science* **2005**, *307*, 555.
(50) Grabow, L. C.; Hvolbæk, B.; Nørskov, J. K. *Top. Catal.* **2009**, *53*, 298.
(51) GGA-PW91 DFT calculations are known to not accurately describe gas phase energies, but a correction of the total energy of −0.6 eV for CO and +0.2 eV for HCOOH reproduces handbook values for a variety of relevant overall gas phase reactions correctly (see Supporting Information).
(52) Grabow, L. C.; Gokhale, A. A.; Evans, S. T.; Dumesic, J. A.; Mavrikakis, M. *J. Phys. Chem. C* **2008**, *112*, 4608.
(53) Nørskov, J. K.; Bligaard, T.; Logadottir, A.; Bahn, S.; Hansen, L. B.; Bollinger, M.; Bengaard, H.; Hammer, B.; Sljivancanin, Z.; Mavrikakis, M.; Xu, Y.; Dahl, S.; Jacobsen, C. J. H. *J. Catal.* **2002**, *209*, 275.
(54) Xu, Y.; Ruban, A. V.; Mavrikakis, M. *J. Am. Chem. Soc.* **2004**, *126*, 4717.
(55) Alcala, R.; Mavrikakis, M.; Dumesic, J. A. *J. Catal.* **2003**, *218*, 178.
(56) Millar, G. J.; Rochester, C. H.; Waugh, K. C. *Catal. Lett.* **1992**, *14*, 289.
(57) Bowker, M.; Hadden, R. A.; Houghton, H.; Hyland, J. N. K.; Waugh, K. C. *J. Catal.* **1988**, *109*, 263.
(58) Waugh, K. C. *Solid State Ionics* **2004**, *168*, 327.
(59) Chinchen, G. C.; Spencer, M. S.; Waugh, K. C.; Whan, D. A. *J. Chem. Soc., Faraday Trans.* **1987**, *83*, 2193.
(60) Neophytides, S. G.; Marchi, A. J.; Froment, G. F. *Appl. Catal., A* **1992**, *86*, 45.
(61) Sakakini, B.; Tabatabaei, J.; Watson, M. J.; Waugh, K. C.; Zemicael, F. W. *Faraday Discuss.* **1996**, 369.
(62) Campbell, C. T.; Daube, K. A. *J. Catal.* **1987**, *104*, 109.
(63) Campbell, C. T.; Koel, B. E.; Daube, K. A. *J. Vac. Sci. Technol., A* **1987**, *5*, 810.
(64) van Herwijnen, T.; de Jong, W. A. *J. Catal.* **1980**, *63*, 83.
(65) van Herwijnen, T.; Guczalski, R. T.; de Jong, W. A. *J. Catal.* **1980**, *63*, 94.
(66) Edwards, J. F.; Schrader, G. L. *J. Phys. Chem.* **1984**, *88*, 5620.

(67) Yatsu, T.; Nishimura, H.; Fujitani, T.; Nakamura, J. *J. Catal.* **2000**, *191*, 423.
(68) Hayden, B. E.; Prince, K.; Woodruff, D. P.; Bradshaw, A. M. *Vacuum* **1983**, *33*, 876.
(69) Edwards, J. F. Ph.D. Thesis, Iowa State University, Ames, Iowa, 1984.
(70) Fujitani, T.; Choi, Y.; Sano, M.; Kushida, Y.; Nakamura, J. *J. Phys. Chem. B* **2000**, *104*, 1235.
(71) Fujitani, T.; Nakamura, I.; Ueno, S.; Uchijima, T.; Nakamura, J. *Appl. Surf. Sci.* **1997**, *121*, 583.
(72) Millar, G. J.; Rochester, C. H.; Howe, C.; Waugh, K. C. *Mol. Phys.* **1992**, *76*, 833.
(73) Nakano, H.; Nakamura, I.; Fujitani, T.; Nakamura, J. *J. Phys. Chem. B* **2001**, *105*, 1355.
(74) Nishimura, H.; Yatsu, T.; Fujitani, T.; Uchijima, T.; Nakamura, J. *J. Mol. Catal., A* **2000**, *155*, 3.
(75) Taylor, P. A.; Rasmussen, P. B.; Ovesen, C. V.; Stoltze, P.; Chorkendorff, I. *Surf. Sci.* **1992**, *261*, 191.
(76) Youngs, T. G. A.; Haq, S.; Bowker, M. *Surf. Sci.* **2008**, *602*, 1775.
(77) Sotiropoulos, A.; Milligan, P. K.; Cowie, B. C. C.; Kadodwala, M. *Surf. Sci.* **2000**, *444*, 52.
(78) Ying, D. H. S.; Madix, R. J. *J. Catal.* **1980**, *61*, 48.
(79) Gao, H. W.; Yan, T. X.; Zhang, C. B.; He, H. *J. Mol. Struct.: THEOCHEM* **2008**, *857*, 38.
(80) Gomes, J. R. B.; Gomes, J. A. N. F. *Surf. Sci.* **1999**, *432*, 279.
(81) Gomes, J. R. B.; Gomes, J. A. N. F. *Surf. Sci.* **2000**, *446*, 283.
(82) Gomes, J. R. B.; Gomes, J. A. N. F. *Surf. Sci.* **2001**, *471*, 59.
(83) Morikawa, Y.; Iwata, K.; Terakura, K. *Appl. Surf. Sci.* **2001**, *169*, 11.
(84) Hayden, B. E.; Prince, K.; Woodruff, D. P.; Bradshaw, A. M. *Surf. Sci.* **1983**, *133*, 589.
(85) Bönicke, I. A.; Kirstein, W.; Thieme, F. *Surf. Sci.* **1994**, *309*, 177.
(86) Carley, A. F.; Roberts, M. W.; Strutt, A. J. *J. Phys. Chem.* **1994**, *98*, 9175.
(87) Fisher, I. A.; Bell, A. T. *J. Catal.* **1997**, *172*, 222.
(88) Schumacher, N.; Andersson, K.; Grabow, L. C.; Mavrikakis, M.; Nerlov, J.; Chorkendorff, I. *Surf. Sci.* **2008**, *602*, 702.
(89) Solymosi, F. *J. Mol. Catal.* **1991**, *65*, 337.
(90) Rodriguez, J. A.; Clendening, W. D.; Campbell, C. T. *J. Phys. Chem.* **1989**, *93*, 5238.
(91) Nakamura, J.; Rodriguez, J. A.; Campbell, C. T. *J. Phys.: Condens. Matter* **1989**, *1*, Sb149.
(92) Rasmussen, P. B.; Taylor, P. A.; Chorkendorff, I. *Surf. Sci.* **1992**, *270*, 352.
(93) Hadenfeldt, S.; Benndorf, C.; Stricker, A.; Towe, M. *Surf. Sci.* **1996**, *352*, 295.
(94) Millar, G. J.; Newton, D.; Bowmaker, G. A.; Cooney, R. P. *Appl. Spectrosc.* **1994**, *48*, 827.
(95) Bowker, M.; Madix, R. J. *Surf. Sci.* **1981**, *102*, 542.
(96) Millar, G. J.; Rochester, C. H.; Waugh, K. C. *J. Chem. Soc., Faraday Trans.* **1991**, *87*, 1491.
(97) Ortelli, E. E.; Weigel, J. M.; Wokaun, A. *Catal. Lett.* **1998**, *54*, 41.
(98) Weigel, J.; Koeppel, R. A.; Baiker, A.; Wokaun, A. *Langmuir* **1996**, *12*, 5319.
(99) Yang, Y.; Mims, C. A.; Disselkamp, R. S.; Kwak, J.-H.; Peden, C. H. F.; Campbell, C. T. *J. Phys. Chem. C* **2010**, *114*, 17205.
(100) Ostrovskii, V. E. *Khim. Tverd. Topl.* **2002**, *1*, 59.
(101) Wachs, I. E.; Madix, R. J. *Surf. Sci.* **1979**, *84*, 375.
(102) Nerlov, J.; Chorkendorff, I. *Catal. Lett.* **1998**, *54*, 171.
(103) Gomes, J. R. B.; Gomes, J. A. N. F. *Electrochim. Acta* **1999**, *45*, 653.
(104) Wachs, I. E.; Madix, R. J. *J. Catal.* **1978**, *53*, 208.
(105) Sexton, B. A.; Hughes, A. E.; Avery, N. R. *Appl. Surf. Sci.* **1985**, *22*−*3*, 404.
(106) Bryden, T. R.; Garrett, S. J. *J. Phys. Chem. B* **1999**, *103*, 10481.
(107) Tang, Q.-L.; Hong, Q.-J.; Liu, Z.-P. *J. Catal.* **2009**, *263*, 114.
(108) Sakong, S.; Gross, A. *J. Phys. Chem. A* **2007**, *111*, 8814.
(109) Edwards, J. F.; Schrader, G. L. *J. Catal.* **1985**, *94*, 175.
(110) Clarke, D. B.; Bell, A. T. *J. Catal.* **1995**, *154*, 314.
(111) Weigel, J.; Frohlich, C.; Baiker, A.; Wokaun, A. *Appl. Catal., A* **1996**, *140*, 29.
(112) Hedge, M. S. *Proc. Indian Acad. Sci. (Chem. Sci.)* **1984**, *93*, 373.
(113) Fisher, I. A.; Bell, A. T. *J. Catal.* **1999**, *184*, 357.
(114) Millar, G. J.; Rochester, C. H.; Waugh, K. C. *J. Chem. Soc., Faraday Trans.* **1992**, *88*, 3497.
(115) Sexton, B. A.; Hughes, A. E.; Avery, N. R. *Surf. Sci.* **1985**, *155*, 366.
(116) Fan, L.; Sakaiya, Y.; Fujimoto, K. *Appl. Catal., A* **1999**, *180*, L11.
(117) Tsubaki, N.; Zeng, J.; Yoneyama, Y.; Fujimoto, K. *Catal. Commun.* **2001**, *2*, 213.
(118) Tsubaki, N.; Ito, M.; Fujimoto, K. *J. Catal.* **2001**, *197*, 224.
(119) Zeng, J.; Fujimoto, K.; Tsubaki, N. *Energy Fuels* **2001**, *16*, 83.
(120) Tsubaki, N.; Fujimoto, K. *Top. Catal.* **2003**, *22*, 325.
(121) Yu, K. M. K.; Yeung, C. M. Y.; Tsang, S. C. *J. Am. Chem. Soc.* **2007**, *129*, 6360.
(122) Muhler, M.; Nielsen, L. P.; Tornqvist, E.; Clausen, B. S.; Topsøe, H. *Catal. Lett.* **1992**, *14*, 241.
(123) Koryabkina, N. A.; Phatak, A. A.; Ruettinger, W. F.; Farrauto, R. J.; Ribeiro, F. H. *J. Catal.* **2003**, *217*, 233.
(124) Sauer, J.; Ugliengo, P.; Garrone, E.; Saunders, V. R. *Chem. Rev.* **1994**, *94*, 2095.
(125) Chakarova-Käck, S. D.; Schröder, E.; Lundqvist, B. I.; Langreth, D. C. *Phys. Rev. Lett.* **2006**, *96*, 146107.
(126) Campbell, C. T. *Top. Catal.* **1994**, *1*, 353.
(127) Calverley, E. M.; Smith, K. J. *Ind. Eng. Chem. Res.* **1992**, *31*, 792.
(128) Cai, J.; Liao, Y.; Chen, H.; Tsai, K. R. *Stud. Surf. Sci. Catal.* **1993**, *75*, 2769.
(129) Yang, Y.; Mims, C.; Disselkamp, R.; Peden, C.; Campbell, C. *Top. Catal.* **2009**, *52*, 1440.
(130) Schumacher, N.; Andersson, K. J.; Nerlov, J.; Chorkendorff, I. *Surf. Sci.* **2008**, *602*, 2783.
(131) Sun, Q.; Liu, C.-W.; Pan, W.; Zhu, Q.-M.; Deng, J.-F. *Appl. Catal., A* **1998**, *171*, 301.
(132) Haldor Topsøe, A/S http://www.topsoe.com/Business_areas/Ammonia/Processes/~/media/PDF%20files/CO_conversion/Topsoe_low_temp_cat_lk%20series.ashx.
(133) Rostrup-Nielsen, J.; Nørskov, J. *Top. Catal.* **2006**, *40*, 45.
(134) Peter Ferrin (private communication) 2007.
(135) Burch, R.; Chappell, R. J. *Appl. Catal.* **1988**, *45*, 131.
(136) Nerlov, J.; Sckerl, S.; Wambach, J.; Chorkendorff, I. *Appl. Catal., A* **2000**, *191*, 97.
(137) Liu, G.; Willcox, D.; Garland, M.; Kung, H. H. *J. Catal.* **1985**, *96*, 251.
(138) Liu, G.; Willcox, D.; Garland, M.; Kung, H. H. *J. Catal.* **1984**, *90*, 139.
(139) Fisher, I. A.; Woo, H. C.; Bell, A. T. *Catal. Lett.* **1997**, *44*, 11.
(140) Bourzutschky, J. A. B.; Homs, N.; Bell, A. T. *J. Catal.* **1990**, *124*, 73.